Alma Mater Studiaorum - Università di Bologna

Dottorato di Ricerca in
Meccanica e Scienze Avanzate dell Ingegneria
Disegno e Metodi dell'Ingegneria Industriale
e Scienze Aerospaziali

Ciclo *XXVII*

Settore Concorsuale di Afferenza: 09/A1 - Ingegneria Aerospaziale
Settore Scientifico Disciplinare: ING-IND/03 - Meccanica del volo

Design and Prototyping High Endurance Multi-Rotor

Coordinatore del Dottorato
Chia.mo Prof. Vincenzo Parenti Castelli

Presentata da:
Mauro Gatti

Relatore
Chia.mo Prof. Fabrizio Giulietti

Esame Finale - Anno 2015

Theory is when we know everything but nothing works.
Praxis is when everything works but we do not know why.
We always end up by combining theory with praxis:
nothing works and we do not know why.

Albert Einstein

Acknowledgments

This thesis is submitted in partial fulfillment of the requirements for the Doctor of Philosophy in Advanced Mechanics and Sciences of Engineering: Design and Methods of Industrial Engineering'. The work has been carried out under the supervision of Prof. Fabrizio Giulietti.

I would like to thank Prof. Fabrizio Giulietti for his guidance during the research work and all the other people that work inside that strange place that is the Flight Mecanics Laboratory.

Mauro Gatti
May 2015, Forlì, Italy

Summary

The topic of this thesis focus on the preliminary design and the performance analysis of a multirotor platform. A multirotor is an electrically powered Vertical Take Off (VTOL) machine with more than two rotors that lift and control the platform. Multirotor are agile, compact and robust, making them ideally suited for both indoor and outdoor application especially to carry-on several sensors like electro optical multispectral sensor or gas sensor. The main disadvantage is the limited endurance due to heavy Li-Po batteries and high disk loading through the use of different small propellers. At the same time, the design of the multirotor does not follow any engineering principle but it follow the ideas of amateurs' builder. An adaptation of the classic airplane design theory for the preliminary design is implemented to fill the gap and detailed study of the endurance is performed to define the right way to make this kind of VTOL platforms.

Contents

List of Figures

List of Tables

Nomenclature

List of Symbols

A_t	Total Disk Area
C	Battery Capacity
C_0	Effective Initial Battery Capacity
C_p	Power Coefficient
C_t	Thrust Coefficient
$f; FM$	Figure of Merit
i	Current Intensity
k	Peukert Coefficient
K_v	Speed Constant
n	Number of rotors
P_{act}	Actual Power
P_{ap}	Power Required for autopilot and payload
P_{pl}	Power Required for payload
P_r	Power Required
$P_{r_{tot}}$	Total Power Required
P_h	Power Required in hovering Condition
q	Dynamic Pressure
R_t	Battery Hour Rating (in hours)
t	Time
T	Rotor Thrust

List of Symbols

$v, \mathcal{V}$	Battery Voltage
V_i	Induced Velocity
W_b	Battery Weight
W_e	Empty Weight
W_{eo}	Operative Empty Weight
$W_{el_{sys}}$	Electronic System Weight
W_p	Payload Weight
W_{pp}	Power Plant Weight
W_{to}, W_0	TakeOff Gross Weight

Greek symbols

ρ	Air density at z
η_b	Effectve Battery Capacity Ratio
η_e	Elictrical Efficiency
η_m	Mechanical Efficiency
η_p	Propeller Efficiency
Ω	Rotatio Rate

Acronyms

BLOS	Beyond Visual Line-Off-Sight
BRLOS	Beyond Radio Line-Off-Sight
COM SP	COMmunication Service Provider
CS-LUAS	Certification Specifications for Light Unmanned Aircraft
CS-LURS	Certification Specifications for Light Unmanned Rotorcraft
EASA	European Aviation Safety Agency
ENAC	Enta Nazinale per l' Aviazione Civile
GPS	Global Position System
IMU	Inertial Measuring Unit
JARUS	Joint Authorities for Rulemaking on Unmanned Systems
LED	Light Emission Diode
MC	Main Controller
MTOW	Maximum Take Off Weight
PMU	Power Management Unit
RLOS	Radio Line-Off-Sight
RPAS	Remotely Piloted Aerial Systems
TLS	Tolerable Level of Safety
VLOS	Visual Line-Of-Sight
VTOL	Vertical take Off and Landing

CHAPTER 1

Introduction

1.1 Motivation

The interest in electrically powered Remotely Piloted Aerial Systems (RPAS) among industry and academia has shown a steep increase along the last decade. This is mostly due to the potentiality of such platforms to play a leading role within a wide range of applications in the field of aerial photography and 3D reconstruction [1], search and rescue [2] and risk management, natural landscape monitoring, and disaster prevention [3]. In particular, among the available fixed and rotary-wing configurations, multi-rotor platforms gained a particular relevance, thanks to the simple configuration, simplicity of use (also in confined spaces), and hovering and vertical take-off and landing capability, which all make them an interesting alternative to fixed-wing aircraft in many practical applicative scenarios.. Also, with respect to a conventional helicopter, a multi-rotor shows an increased manoeuvrability and a faster response to external disturbances together with a more compact size. This is achieved by spreading the total disc area into multiple rotor units. Thus, to provide the required thrust, smaller propellers rotating at higher speed are employed, at the cost of a loss in efficiency with respect to the conventional, single rotor configuration. This, in addition to the limited duration/weight ratio typical of electrically driven systems, makes the endurance in the hovering condition a critical, but challenging, issue in the framework of the multi-rotor platform design process.

1.2 Literature Review and Thesis Objectives

Studies addressing electric aircraft performance and became available only in last few years. Recent works present results related to fixed-wing aircraft, where the effects of Peukert's law on the available battery capacity are taken into account. In Refs. [4] and [5], the best range condition is derived, whereas in Ref. [6] endurance estimates are validated by means of an experimental investigation. With respect to multi-rotor platforms, Ref. [7] presents a novel configuration where endurance is increased by using higher diameter propellers for lift generation and smaller propellers for attitude control, whereas in Ref. [10] the authors present an application of a statistically-based sizing methodology to multi-rotor RPAS, allowing for the estimation of the gross take-off weight as a function of hovering time and payload requirements, through the analysis of available data from platforms currently on the market. This thesis presents the analytical study of battery-powered rotary-wing aircraft endurance in hovering flight condition, and its experimental validation carried out by using a multi-rotor platform. Starting from the balance equation of required and available power, and by taking into account airframe features, rotor figure of merit, and payload required power, two main results are obtained and discussed: 1) an analytical model for accurate estimate of hovering time as a function of on-board battery capacity, and 2) a set of approximate solutions for deriving the best endurance condition in terms of optimum capacity and maximum achievable hovering time for the cases when the figure of merit can be assumed to be constant, and the power required by the payload is small if compared to the hovering power. The problem of hovering flight time is addressed and approximate analytical models describing the best endurance condition are derived. In the Result section numerical simulations and flight testing campaign data, validating the effectiveness of the proposed approach, are presented.

1.3 Outline

The work is divided into three main parts. The first part,(Chapter 2), describe the platform in its main parts. Second part,(Chapter 3), copes with the adaptation of the classic airplane design methodology already used for airplane and helicopters.Third part, (Chapter 4), a detailed study about endurance performance is developed in relation to the configuration of the platform. In particular, a closed analytical solution is proposed and verified through practical experiments with a flying test bench.

CHAPTER 2

System Description

The following paragraph describe the platform studied during the three years of the PhD. The short description contain physical and mechanical aspects and the basic theory about generation of thrust for a rotor in single and coaxial configuration through the momentum theory.

2.1 Multi-Rotor platforms

Multi-rotors are a VTOL aircraft where the general term encompassing not only quad-rotor but also tri-rotor, hexa-rotor, octo-rotor and all other form of rotorcraft with more than 2 propellers/rotors. The very first experimental attempts of taking off with a rotor-craft were mostly done with multirotors. Around 1907 Jacques and Louis Breguet, French brothers, built and tested Gyroplane, a quadcopter. They managed take-off, although the design proved to be very unstable and hence impractical. In 1924 French engineer Étienne Oehmichen flew his quadcopter (Fig.2.1) a distance of 360 m setting a world record.

In the same year he flew a 1km in 7m and 40s. Around the same time George de Bothezat built and tested his quadrotor for the US army (Fig.2.2), completing a number of test flights before the program was scrapped.

These type of vehicle typically had a central engine housed centrally in the fuselage, driving the 4 rotors via belts or shafts. Belts and shafts however are heavy and importantly, subject to breakage. A quad-rotor is not naturally stable because is, in terms of control variables, an under actuated vehicle where four control variables are present to control six

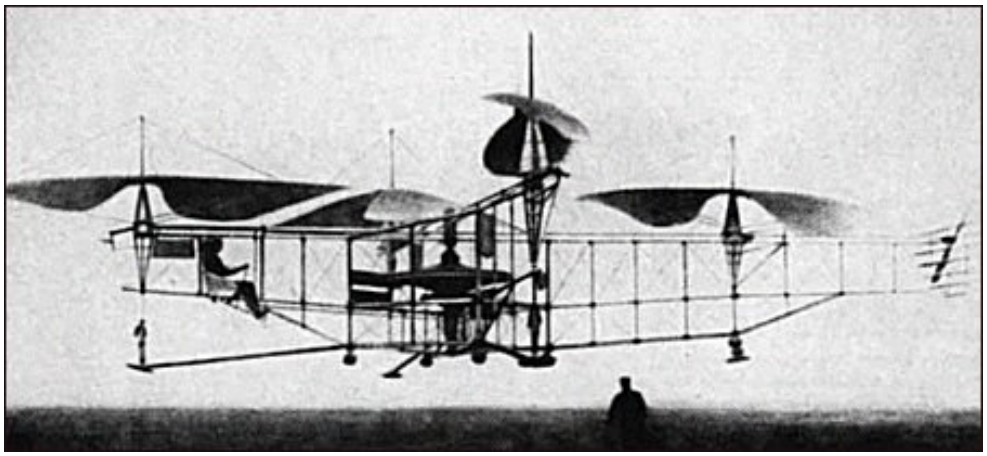

Figure 2.1: Oehmichen Quadrotor

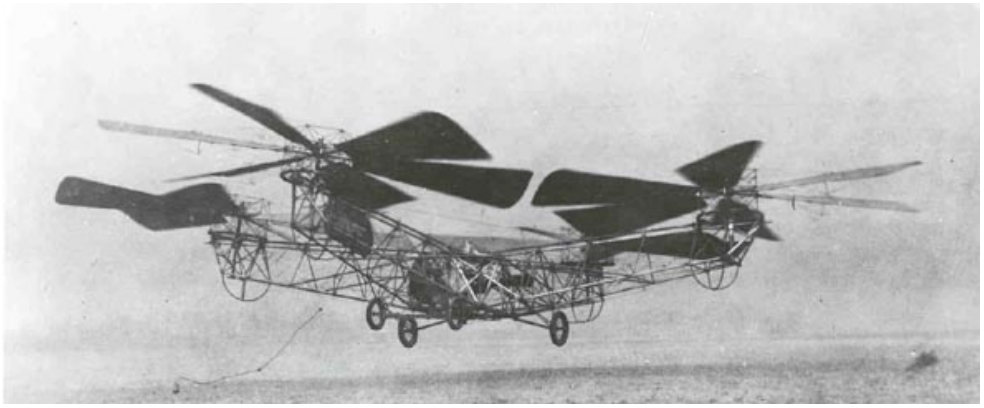

Figure 2.2: Bothezat Quadrotor

mechanical degrees of freedom. In the absence of computers, this meant a monumental workload for the pilot. As a result, multi-rotors designs were abandoned in favor of single, or on rare occasions for very large transport helicopters, double rotor designs.

With the advent of electric motors and especially microelectronics and micro-mechanical devices, a few years ago it became possible to build reliable and efficient multi-rotors. Modern multi-rotor have an electric motor mated to each rotor, sitting directly below or above it. A flight computer constantly monitors the orientation of the copter and corrects for instability by changing not the pitch of the rotors but simply the rpm of the individual motors/rotors. This fixed pitch design is much simpler than the complex swashplate mechanics that are required for single rotor helicopters.

The quad-rotor, features two pair of rotors mounted at the end of a simple cross-shaped structure, or at the corners of a square frame. Two rotors rotate in the clockwise direction and two rotate counter-clockwise, such that at hover each rotor produce a thrust equivalent to one fourth of the vehicle weight, with zero pitch and roll moments and perfectly balanced rotor aerodynamic yawing torques.Yaw control is achieved unbalancing aerodynamic torques acting on the two pairs of rotors (i.e. increasing the speed of clockwise rotors while decreasing the rotation rate of the other two, or viceversa), keeping a constant total thrust. Roll and pitch moment are obtained by variation of lateral and longitudinal rotor thrust, respectively (i.e. increasing the forward rotor rotation rate while decreasing that of the aft-mounted rotor, a pitch-up moment is obtained) (Fig.2.3).

To compute the aerodynamic forces generated by rotors, and needed to the further performance calculations, it is possible use the results of the classic momentum theory (MT) and the more detailed blade element theory (BET) [11]. The induced rotor velocity, by assumption, is constant on the whole area of the disk actuator. the air is considered incompressible. The thrust (T), generated by rotors, is linked to the induced velocity (v_i), as the thrust coefficient (C_T) to the inflow ratio (λ_i) (2.1, 2.2).

$$T = 2\rho A v_i \sqrt{u_R^2 + (w_R - v_i)^2} \tag{2.1}$$

$$C_T = \frac{T}{\rho A V_{tip}^2} \tag{2.2}$$

Rearranging equation 2.1 the induced velocity, in hovering condition, can be expressed as:

$$v_i = \sqrt{\left(\frac{T}{A}\right)\frac{1}{2\rho}} \tag{2.3}$$

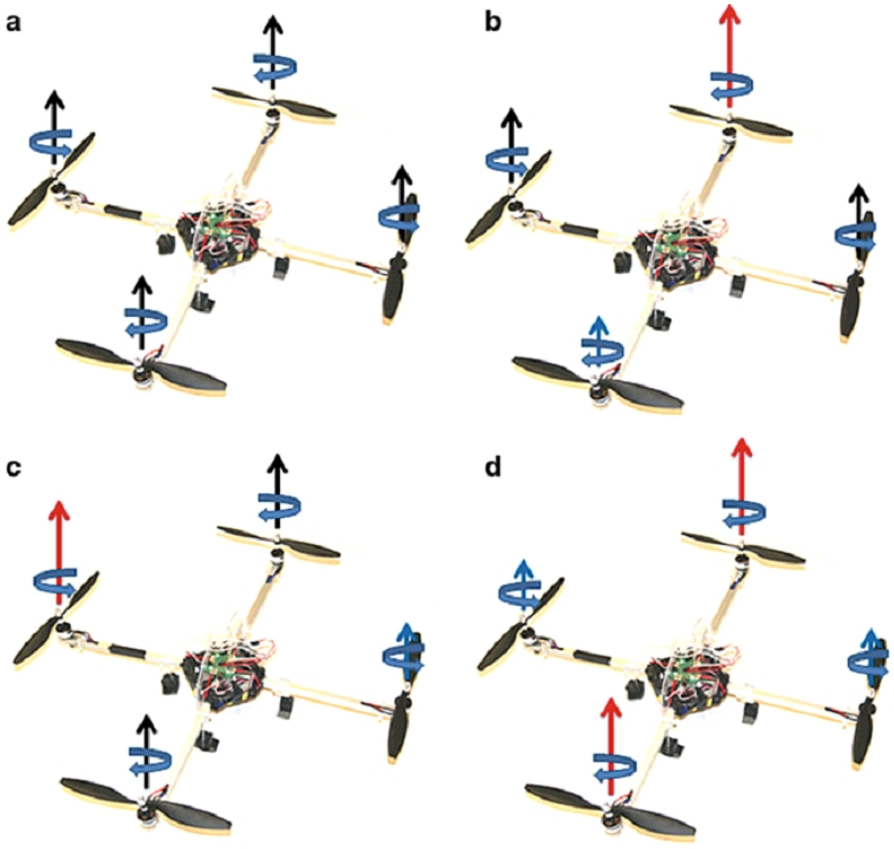

Figure 2.3: Quadrotor movements: (a) hover, (b) roll, (c) pitch, and (d) yaw

So, the power required to hover condition, on the time rate-of-work done by the rotor on the fluid per unit thrust, is given by:

$$P_h = \frac{T^{\frac{3}{2}}}{\sqrt{2\rho A}} \tag{2.4}$$

This power is also called ideal power because it is entirely induced in nature without consider the contribution of viscous effect of the fluid. using the modified form of the MT, with non ideal approximation for the power, it is possible to write the figure of merit as:

$$FM = \frac{P_{ideal}}{kPideal + P_0} = \frac{\frac{C_T^{3/2}}{\sqrt{2}}}{\frac{kC_T^{3/2}}{\sqrt{2}} + \frac{\sigma C_{d_0}}{8}} \tag{2.5}$$

Where P_0 is the profile power required and k is the coefficient that take into account the induced losses (i.e $k = 1.0$ for ideal induced losses and $k = 1.15$ for non-ideal losses).

2.1.1 Coaxial rotor configuration

In some cases multi-rotor adopt contrarotating coaxial rotor system. In electrical vehicle this application is easier than a mechanical costruction because it is possible make this via two DC motors commuting the poles of the power line (Fig.2.4).

Figure 2.4: Coaxial rotor system

Contrarotating coaxial rotor design has some advantage. One of these is that the net size of the rotors is reduced because each rotor provide vertical thrust [11]. However, the two rotors and their wakes interact with one other and this interacting flow incurs a loss of net rotor system aerodynamic efficiency. Assuming the rotor planes are sufficiently close

together and that each rotor provide an equal fraction of the total system thrust, via the MT is possible describe the induced power for the separate rotors as:

$$P_i = \frac{2T^{3/2}}{\sqrt{2\rho A}} \tag{2.6}$$

The induced power factor k_{int} is considered to be ratio expressed in the following equation:

$$k_{int} = \frac{P_{i_{tot}}}{P_i} = \left(\frac{(2T)^{3/2}}{\sqrt{2\rho A}}\right)\left(\frac{2T^{3/2}}{\sqrt{2\rho A}}\right)^{-1} = \sqrt{2} \tag{2.7}$$

That is the 41% of induced power relative to the power required to operate the two rotors in complete isolation. MT shows a pessimistic analysis if compared with experimental measurements. This is in function of the finite spacing between the two rotors. Through a more detailed analysis of the induced velocity of the two rotors, k_{int} is equal to 1.281, that is the 28%. Under this condition the figure of merit of a coaxial rotor (Fig.2.8) became:

$$FM = \frac{P_{ideal}}{kP_{ideal} + P_0} = \frac{\frac{C_T^{3/2}}{\sqrt{2}}}{\frac{k_{int}kC_T^{3/2}}{\sqrt{2}} + \frac{\sigma C_{d_0}}{8}} \tag{2.8}$$

Where $k_{int} = 1$ for a single isolated rotor.

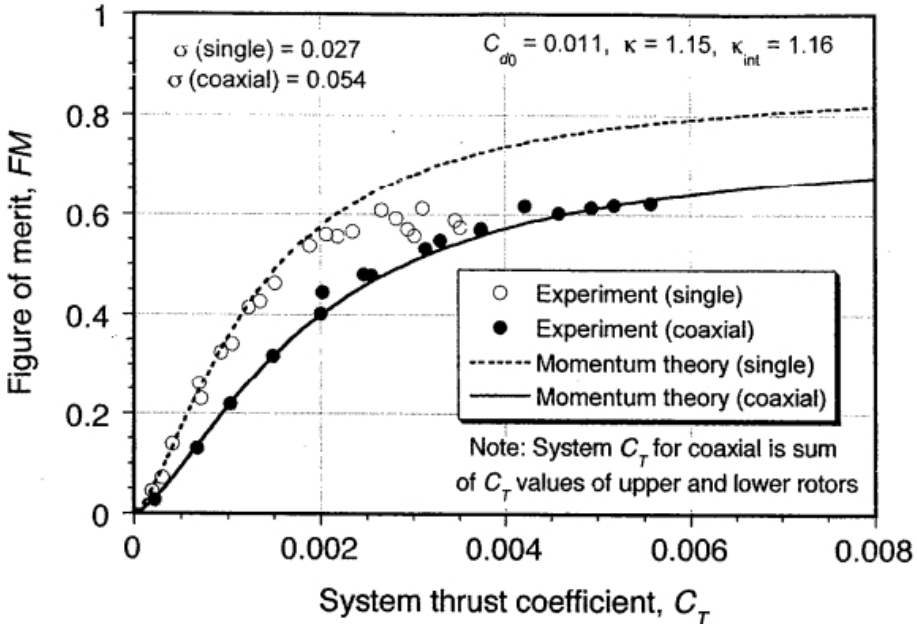

Figure 2.5: FM for a coaxial rotor compared to measurement [11]

Anyway the coaxial configuration maintain also other benefits [23]; the torque of any couple of rotors is always balanced because they work at the same rotational speed with opposite direction. Outside the hovering condition, for example in forward flight, the dissymmetry of lift generated by the advancing rotor blade, is balanced by the effect on the the retreating blade of the contrarotating rotor. Last benefits is a reduction of noise and, in case of helicopter configuration, there is not a tail rotor that that wastes a part of available engine power that would be devoted to lift and thrust.

2.2 Driving System

Conventional platform are driven by one or more internal combustion engine. In this case engine controls can be added to simple engines in order to improve reliability and fuel consumption. The engine control unit can control throttle servo position, spark timing, cowl flap opening, or fuel injection, depending on engine configuration. Measured engine properties can include shaft rotational angle, rpm, air inlet temperature, exhaust temperature, and cylinder head temperature. These sensors must be added to the engine. Instead, electrical platform are simpler and so DC motors are driven directly by an Electronic Speed Control. Both driving system configurations drive a propeller with two or more blade.

2.2.1 Electric Motors

Electric motors don't have consumables as fuel and lubricants like combustion engine and have poor maintenance. Brushless motors have two main configurations: inner-runner and out-runner. Multi-rotor applications generally use out-runner motor. Out-runners spin much slower than their inner-runner counterparts with their more traditional layout while producing far more torque. This makes an out-runner an excellent choice for directly driving electric aircraft propellers since they eliminate the extra weight, complexity, inefficiency and noise of a gearbox. Also performance characteristics are independent of altitude to a first order; but the real one limitation is the the endurance in flight due to power source.

Modern electrical UAS are small with a weight less than 10 kilograms and they are powered with motors of less than 1 kW. The motor life is limited by the bearing wear.

Electric Motors model

Multi-rotors use DC electric motors. Such motors, featuring high power-to-weight ratio, are widely used for scale-model aircraft, represent a suitable solution for micro/mini UAV

applications. The following assumption are made within the initial sizing process:

- for brushless permanent-magnet motors, the power factor is equal to unit
- Magnetic loss is neglected

Input power (P_{in}) and shaft output power are given by the following expressions:

$$P_{in} = V_{in} \cdot I_{in} \tag{2.9}$$

$$P_{out} = (I_{in} - I_0) \cdot (V_{in} - I_{in} R_a) \tag{2.10}$$

Where I_{in} is the input current, I_0 is the no-load current,V_{in} is the input voltage and R_a is the motor resistance. The global electric system efficiency and the shaft rotational speed (Ω) in function of the motor speed constant (K_V) are given as:

$$\eta_s = \eta_D \cdot \left(1 - \frac{I_{in} \cdot R_a}{V_{in}}\right) \cdot \left(1 - \frac{I_0}{I_{in}}\right) \tag{2.11}$$

$$\Omega = (V_{in} - I_{in} \cdot R_a) \cdot K_V \tag{2.12}$$

Where $\eta_D \approx 0,95$ is the driver efficiency.

For the purposes of the present work more than 2000 DC engine have been selected and classified from Motocalc databases. Fig.2.6 shows the results obtained.

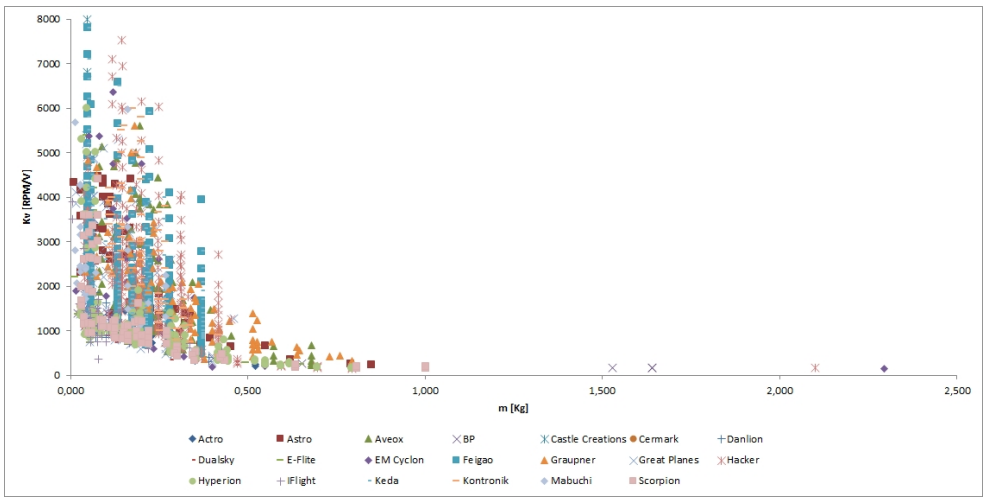

Figure 2.6: Speed Constant (K_v) as a function of motor mass

Among 60 models of motor currently available on the market, 4 different DC motors have been selected with a complete information datasheet.

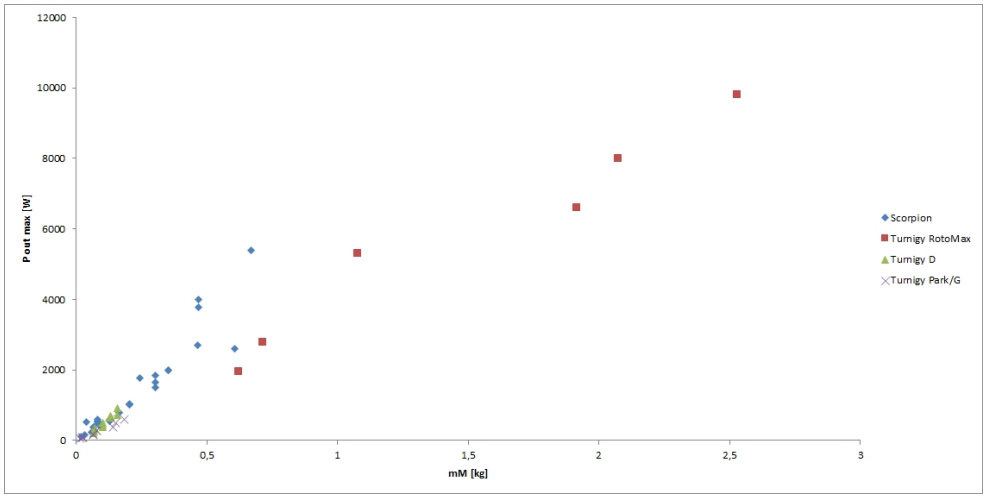

Figure 2.7: Motor maximum output power as a function of motor mass (selection of 4 manufacturers)

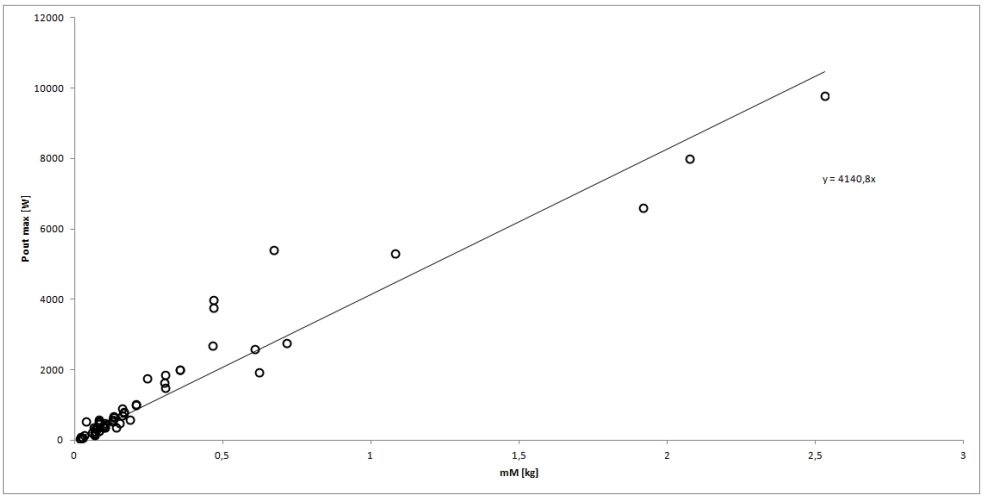

Figure 2.8: Motor maximum output power as a function of motor mass (trend)

We define maximum power-to-mass ratio (B_{PM}) relative to list of 4 DC motors Fig.2.8 into the model as:

$$P_{out_{max}} = B_{PM} \cdot m_M \tag{2.13}$$

That is by the trend line value:

$$P_{out_{max}} = 4140,8 \cdot m_M \tag{2.14}$$

The same procedure is applied for K_V and B_{K_V} (Fig.2.9):

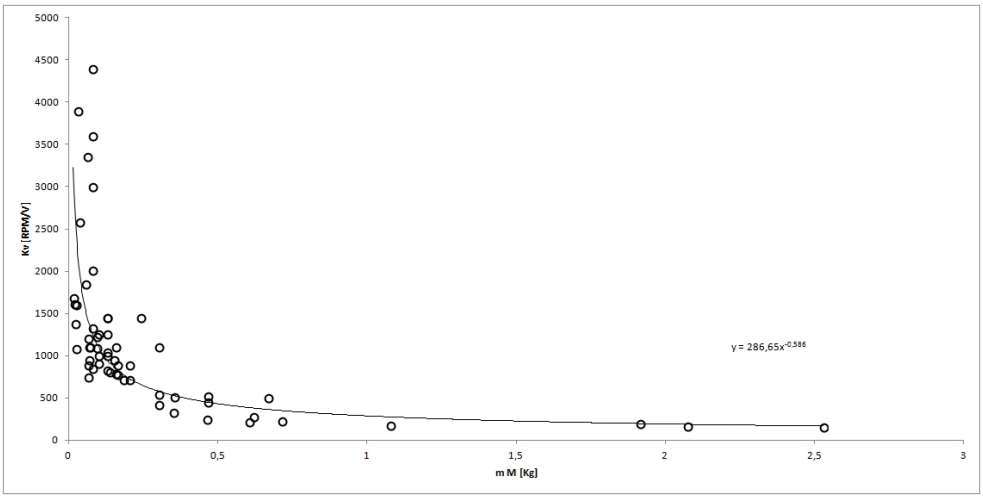

Figure 2.9: Speed constant as a function of motor mass (selection of 4 manufacturers)

$$K_V = B_{K_V} \cdot {m_M}^{-0,586} \tag{2.15}$$

$$K_V = 286.5 \cdot {m_M}^{-0,586} \tag{2.16}$$

The expression that links the max P_{out} to the mass of the motor m_M can be used to estimate the DC engine weight.

2.2.2 Electronic Speed Control (ESC)

DC motor speed is controlled by a motor controller called ESC. The function of the ESC is to vary the to vary the voltage that is applied to the motor and consequentially change the rotational speed. The ESC's choice is function of the maximum current of the motor

Data available online at http://www.motocalc.com/ [retrived April 2012]

driven. Generally the user have to take an ESC that can menage a current of $10 - 20\%$ more than the maximum motor current. The power of an ESC [15] can be defined as:

$$P_{esc} = \frac{I_{mot} \cdot V_{mot}}{\eta_{esc}} \tag{2.17}$$

The ESC efficiency (η_{esc}) is maximum when the power setting of the motor is near of the 100%. The efficiency information for ESC is not available from the manufactures, but it can be defined wit a value of $85\% - 95\%$.

To define a database of ESC main characteristics it is take into account only one main manufacturer (Turnigy) that allow info. With the database we can define two plot where continuous current, Fig.2.10, and volume expressed in mm^3, Fig.2.11, are in function of the ESC mass.

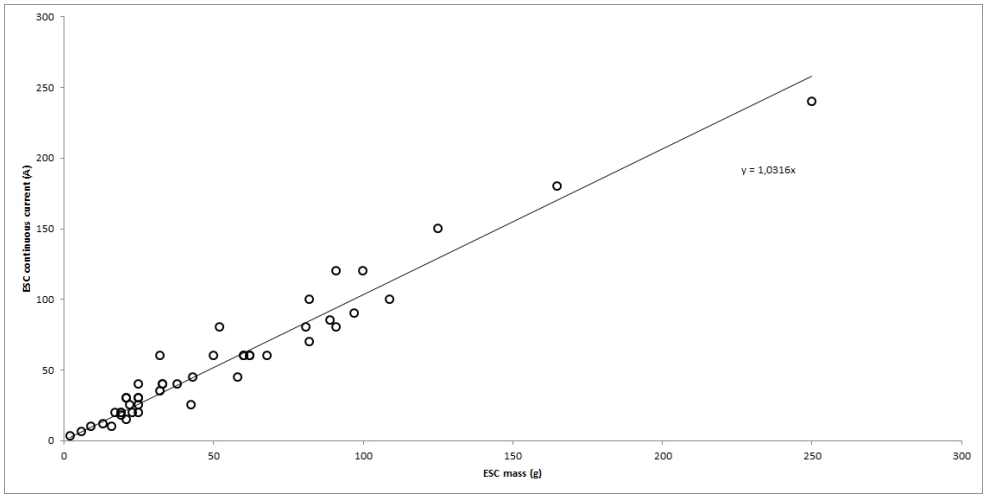

Figure 2.10: ESC cont. current vs mass

The relation between the ESC parameters are defined by the following linear equations:

$$Cont_{curr} = 1,0316 \cdot mass_{esc} \tag{2.18}$$

$$Vol_{esc} = 617,31 \cdot mass_{esc} \tag{2.19}$$

2.2.3 Propeller

Propeller performance at low Reynolds numbers has become increasingly important in the design and performance prediction of RPSs. Generally a two blade type, with variable

http://www.turnigy.com/

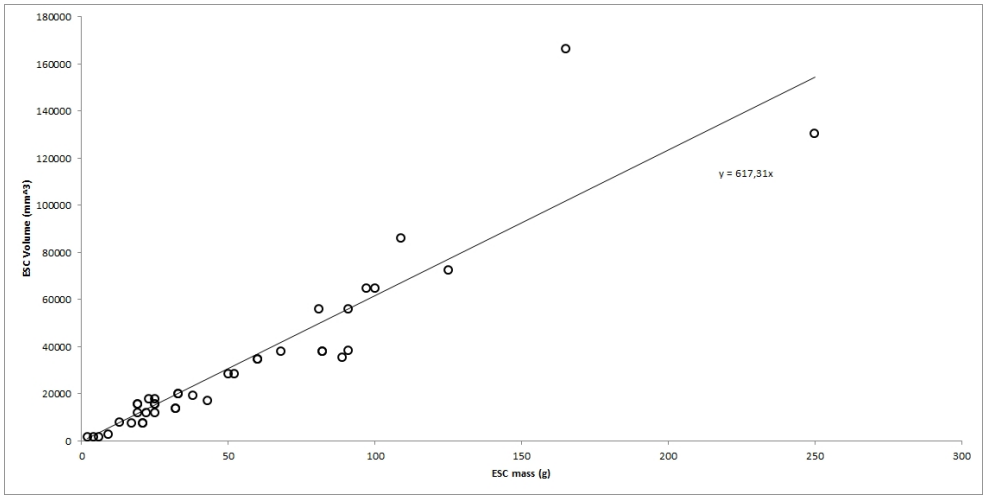

Figure 2.11: ESC volume vs mass

diameter, in plastic or carbon fiber are widely used. The principal limit of these propeller is the short diameter that have a negative influence on aerodynamic characteristics reducing efficiency. The maximum average propeller efficiency is about 0.5 to 0.7 as shows, for example, in Fig.2.12 relatives of a Graupner 11x8 propeller [21].

Propeller used for the experiment is a $T - Motor13x4.4CarbonV2$. This lightweight propeller is make to allow high strength with less inertia and prolong hovering time in relation to high efficiency. Sadly, T-Motor do not provide aerodynamic characteristic that are been obtained through a test banch.

2.3 Batteries

The device that convert electrochemical energy into electrical power is the battery. Battery can be rechargeable and not. Not rechargeable are also called primary or single use. The first type have high performance than rechargeable but the cost of replacing is not convenience for a multi-use RPV as the multi-rotors.Several battery chemistries have been used for UAS propulsion systems. The properties of several battery types are shown in Tab.2.1. Nickelcadmium (NiCd) batteries were dominant in the 1980s and 1990s. Nickel metal hydride (NiMH) made a brief appearance in the late 1990s and early 2000s. However, lithium-ion (Li-Ion) and lithium-ion-polymer (Li-Po) batteries are the main type in use today for small UAS/RPAS propulsion systems. Lithium sulfur (LiS) promises to provide improved performance once more fully matured.

The second step in the preliminary sizing process for conventional aircraft is the fuel

$http://www.rctigermotor.com/html/2013/prop_0904/31.html$

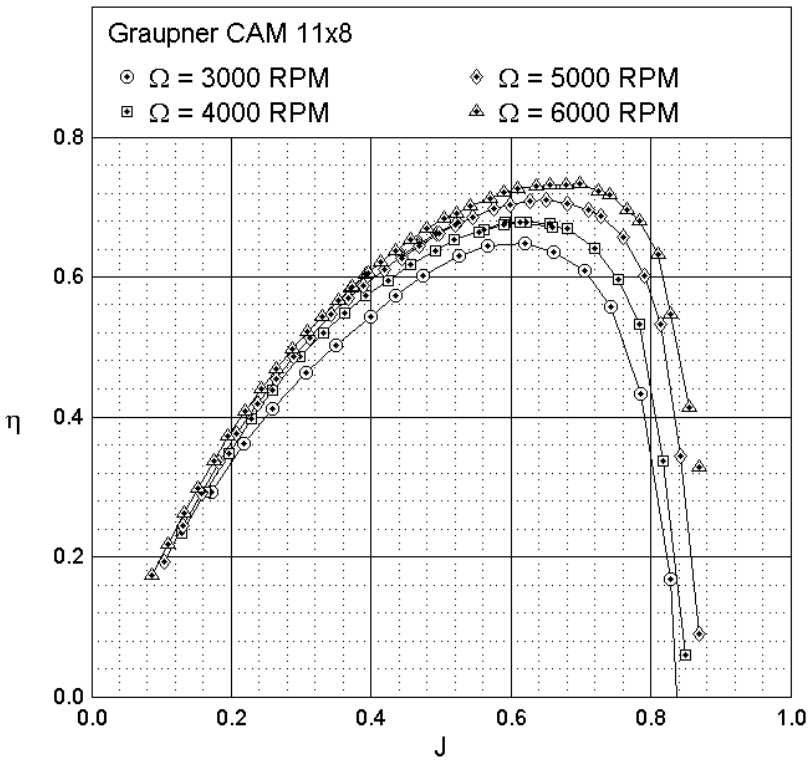

Figure 2.12: η_p vs J of Graupner 11x8 propeller [21]

Figure 2.13: T-Motor 13x4.4 Carbon V2

fraction required for each mission segment, and thus the Specific Fuel Consumption (SFC) plays a critical role. Electrically powered aircraft shows a different behavior, since the weight remains constant along the whole missions. Currently, battery technology is based on lithium polymer battery providing better performance with respect to previous technologies (NiCd, LiFe). The following batteries parameters [22] are available from manufacturers' data sheets, allowing an estimation of the battery fraction:

1. *Energy or Nominal Energy or Energy Capacity* of the battery (measured in Wh for a specific C-rate): is the total Watt-hours available when the battery is discharging given a certain discharge current (specified as a C-rate) from100 percent state-of-charge to the cut-off voltage. Energy is calculated by multiplying the discharge power (in Watts) by the discharge time (in hours). Like capacity, energy decreases with increasing C-rate.

2. *Depth of Discharge* (DOD - measured in %): is the percentage of battery capacity that has been discharged expressed as a percentage of maximum capacity. A discharge to at least 80 % DOD is referred to as a deep discharge. The cycle life of a battery is the number of discharge-charge cycles before fails in function of temperature and humidity. High DOD generally define a low cycle of life.

3. *Specific Energy* (measured in Wh/kg): is the nominal battery energy per unit mass, sometimes referred to as the gravimetric energy density. It is a characteristic of the

battery chemistry and packaging. Along with the energy consumption of the vehicle, it determines the battery weight required to achieve a given electric range.

4. *Energy Density* (measured in Wh/L): is the nominal battery energy per unit volume, sometimes referred to as the volumetric energy density. It is a function of the battery chemistry and packaging. Along with the energy consumption of the vehicle, it determines the battery size required to achieve a given electric range.

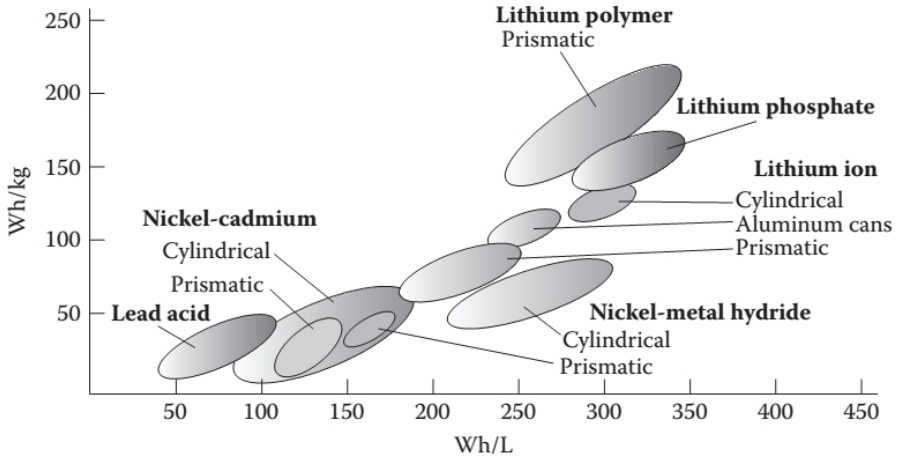

Figure 2.14: Specific Energy vs Energy density for several type of battery [28]

Battery	Specific Energy	Practical Specific Energy	Specific Power	Cell Voltage
[Type]	$[Wh/kg]$	$[Wh/kg]$	$[W/kg]$	$[V]$
$Pb/acid$	170	$30-50$	180	$1,2$
$NiCd$	240	60	150	$1,2$
$NiMH$	470	$23-85$	$200-400$	$0,94-1.2$
$Li-Ion$	700	$100-135$	$250-340$	$3,6$
$Li-Po$	735	$50,7-220$	$200-1900$	$3,7$
$Li-S$	2550	350	$600-700$	$2,5$

Table 2.1: General characteristics of rechargeable Battery Chemistries

It can be notice that the we have best performance for Li-Po and Li-S batteries. The capacity of a battery is the usable energy for the whole system. This energy is defined by

the following parametric equation [15] that scales the battery energy with battery weight and specific energy:

$$E_{nergy_{Batt}} = E_{spec}\frac{W_b}{g} \cdot \eta_b \cdot f_{usable} \tag{2.20}$$

Where η_b is in function of the current draw profile and the f_{usable} or f_{DOD} is factor accounts for the permissible battery pack depth of discharge, which can be a very significant endurance driver. The depth of discharge is the ratio of battery usable energy to the total stored energy. The battery efficiency and permissible depth of discharge depend on battery chemistry and design attributes.

Multi-rotors adopt battery pack arranged in a combination of series and parallel cells. A cell is the basic electrochemical unit providing a source of electrical energy by direct conversion of chemical energy. A cell is an assembly of electrodes, separators, electrolyte, container and terminals [28]; while a battery consist of one or more electrochemical cells connected in an appropriate series (strings) or parallel arrangement to provide a specific required current or voltage level. The type of arrangement is in function of the input motor voltage and the maximum system current required as show in Eq.2.21 and Eq.2.22.

$$V_{batt} = N_{series} \cdot V_{cell} \tag{2.21}$$

$$I_{max,batt} = N_{strings} \cdot I_{max,cell} \tag{2.22}$$

In relation of these the energy battery can be expressed as:

$$E_{batt} = N_{cell} \cdot C_{cell} \cdot V_{cell} \cdot f_{usable} \tag{2.23}$$

Lithium polymer batteries have a voltage per cell that varies between th absolute minimum safe voltage per cell is 3.0 volts, and the maximum is 4.2 volts in function of the technologies used. Multiply these values by the cell count to get the minimum and maximum voltages for a given battery pack as in example in Tab.2.2. As the battery is discharged, the voltage drops gradually and constantly until it reaches 15% charge at a voltage of 3.7 volts. Below this point the voltage drops much more rapidly. Each lithium polymer battery cell also has an internal resistance of around 5 milliohms for a new cell and 20 milliohms for an old cell. The effect of this internal resistance is to cause a significant instantaneous drop in the battery voltage as a function of the actual current draw as in equation 2.24.

$$V_{drop} = I \cdot R_{int} \tag{2.24}$$

Cell Count	Nominal Voltage	Min Voltage	Max voltage
1	3,7	3,0	4,2
2	7,4	6,0	8,4
3	11,1	9,0	12,6
4	14,8	12,0	16,8
5	18,5	15,0	21,0
6	22,2	18,0	25,2

Table 2.2: lythium Polymer Battery Voltage

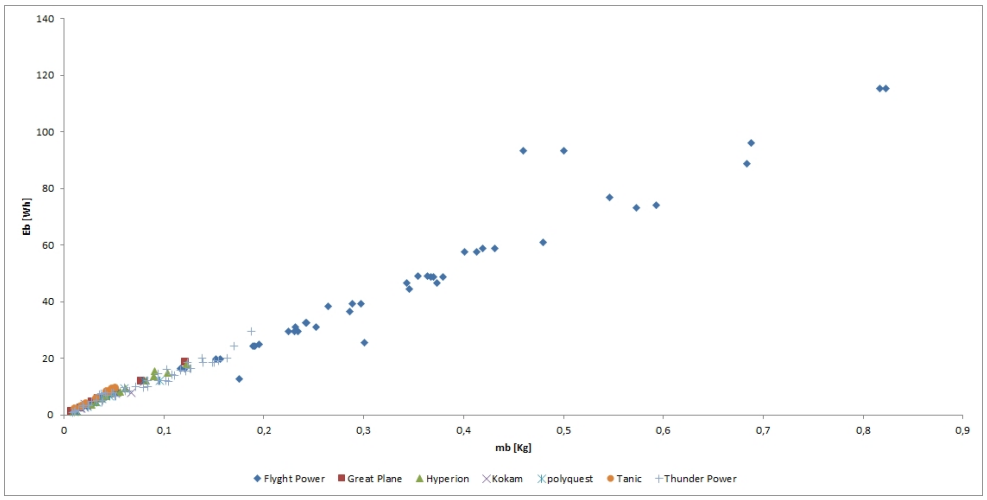

Figure 2.15: Battery capacity as a function of battery mass

A battery set is selected on the basis of a dedicated database [18]. A number of 163 Lithium Polymer batteries from seven main manufacturers have been selected and classified. The relationship between energy capacity, E_b, (expressed in $W \cdot hr$), and battery mass, m_b, is shown in Fig. 2.15.

while Fig. 2.16 shows the trend line that define the relation between the two parameters given by the following equation:

$$E_b = 138,17 \cdot m_b - 0.0422 \tag{2.25}$$

It can be noticed that FlightPower is the manufacturer that produces batteries that allow a wide range of E_b in relation to the m_b. Also its website gives a complete list of data. So FlightPower is been chosen to be analyzed as follow. Fig. 2.17 and Fig. 2.18 show the relation of the parameters with the mass and the volume with their trend line.

Data available online at http//www.flightpower.co.uk/

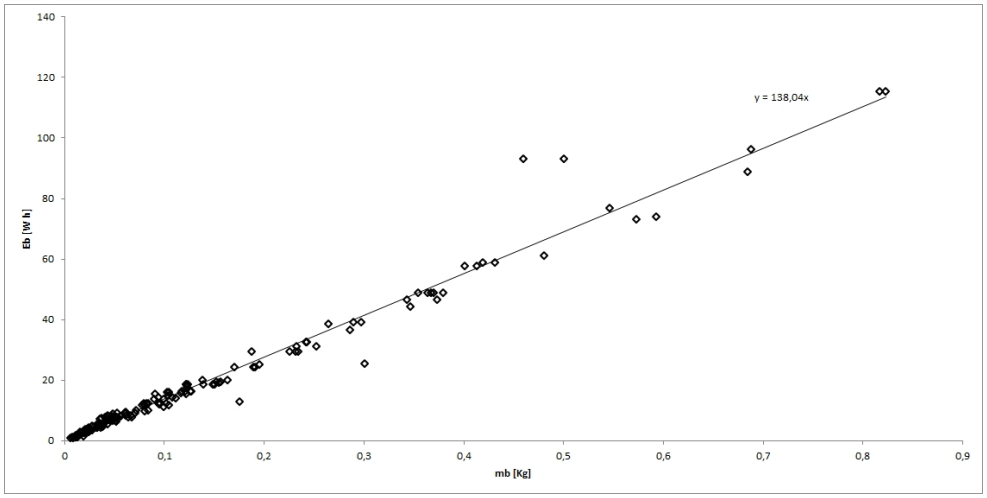

Figure 2.16: Battery capacity as a function of battery mass trend line

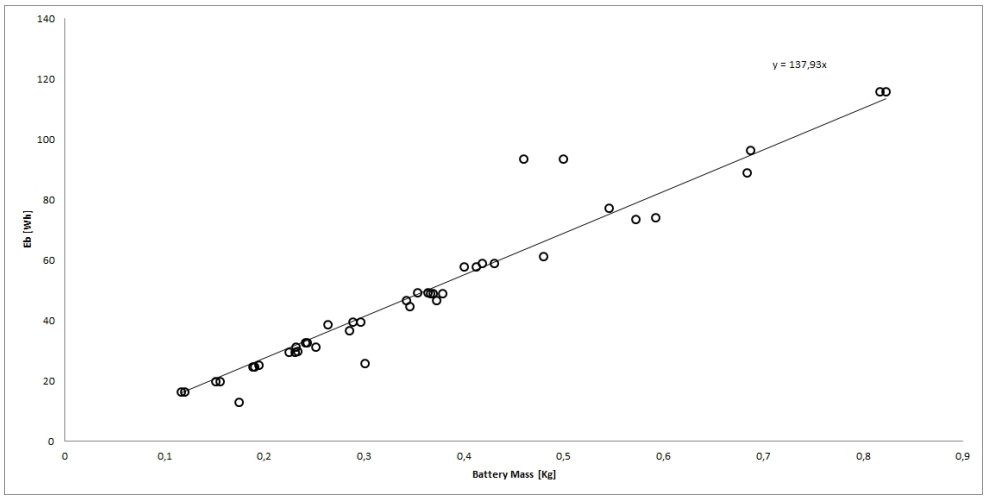

Figure 2.17: Battery capacity as a function of battery mass (FlightPower)

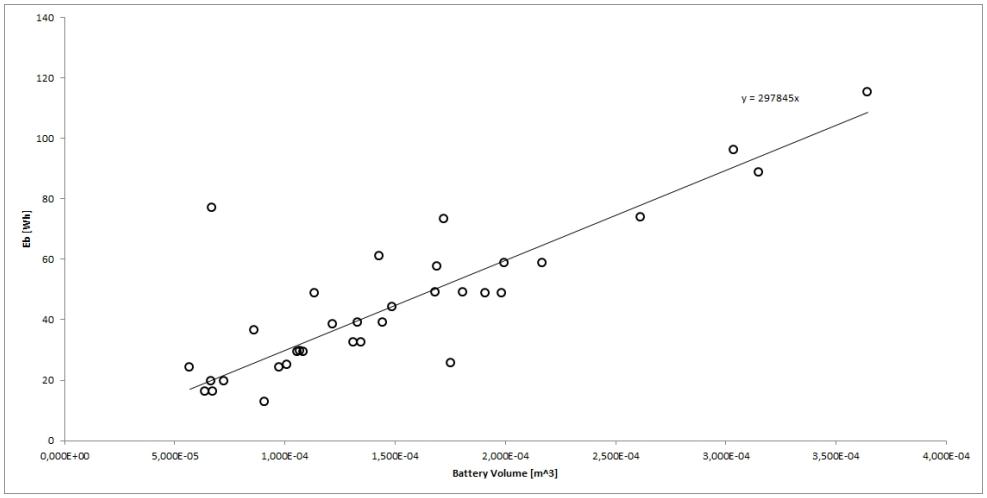

Figure 2.18: Battery capacity as a function of Volume (FlightPower)

The relation defined by trend line are:

$$E_b = 137,93 \cdot m_b \tag{2.26}$$

$$E_b = 297845 \cdot Vol \tag{2.27}$$

2.3.1 Discharge battery model and approximation

In 1963, Shepard [24], define the equation that describe a complete battery discharge for the case when current density distribution is uniform for a Li-Po battery. The battery potential, during the discharge, is given as a function of time, current density, polarization, internal resistance, and other factors (2.28).

$$\mathcal{V} = E_0 - R \cdot i - K\frac{C}{C - it}(it + i^*) + Ae^{(-B \cdot it)} \tag{2.28}$$

Where the two main term are respectively the:

$$Polarization\ Resistance = K\frac{C}{C - it} \cdot i^* \tag{2.29}$$

$$Polarization\ Voltage = K\frac{C}{C - it} \cdot it \tag{2.30}$$

The term A is the exponential zone amplitude (V); B is the exponential zone time constant inverse (Ah^{-1}); R is the internal resistance (Ω); i is the battery current (A),

i^* is the filtered current (A); $it = \int idt$ and K is the polarization constant (V/Ah) or polarization resistance (Ω) [25].

The battery discharge characterization allow to find an experimental value of Peukert coefficient. Via a Programmable DC Electronic Load were performed several tests on the batteries used on-board of the multi-rotor. Four discharge at variable C-rate,from 1 to 4 with a step of 1, were performed. For every battery pack a non complete discharge is achieved. The battery capacity is used for the 80% of the nominal capacity, this is reach when the battery voltage has a drop of $\Delta V \approx 2$ volt. The typical discharge curves of a Li-Po battery are shown in 2.19.

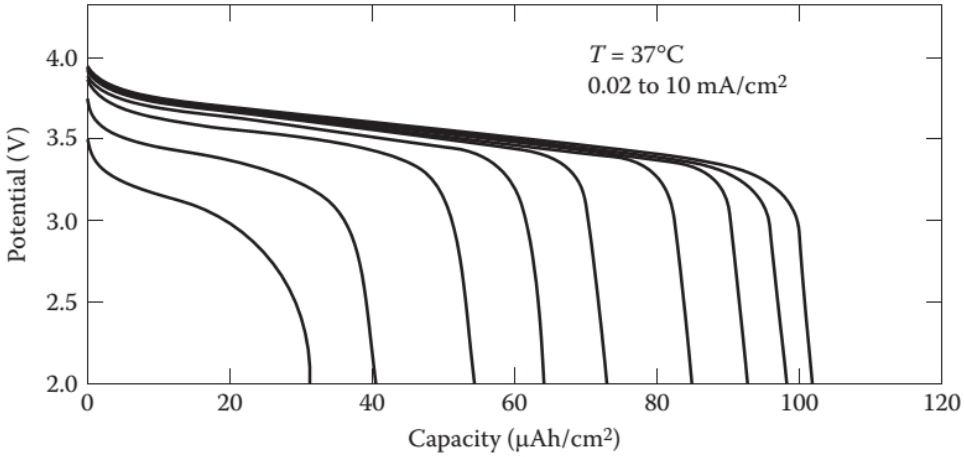

Figure 2.19: Example of Li-Po battery discharge curves [27]

The experimental characterizations of the batteries were obtained via set of battery discharge performed with the electronic load. Electronic properties that are measured include the battery voltage, current and power, while measurement variables are discharge time and capacity. For the experiment four batteries Dualsky 10000mAh $XP100004HED$ type are been used. In order to define physical characteristics, the batteries were weighted in order to calculate their Specific Energy and energy to Volume as show in Ta.2.3.

The results put on evidence that any battery pack have weight difference and so specific energy difference. These difference, however small, have influence in term of capacity and time of discharge. The curves were acquired fixing a constant current of discharge in function of a C-rate. Fig.2.20 and Fig.2.22 show the voltage drop in function of the battery capacity for the battery pack I; while Fig.2.21 and fig.2.23 show the voltage drop in relation of the elapsed time of discharge. All the curves are plotted for different C-rate: from 1C to 4C range.

Maynuo model M97 - www.maynuo.com/

XP100004HED Specification		
Nominal Capacity	10000	mAh
Nominal voltage	14.8	volt
Energy	148.0	$Watt \cdot h$
Number of Cell	4S1P	
Nominal Weight	780	g
Dimensions	167x48x48	mm

Batt. Pack	Weight	Specific Energy	Energy to Volume
n^o	$[g]$	$[Watt \cdot h/g]$	$[Watt \cdot h/mm^3]$
I	774,8	0,1910	$3,846 \cdot 10^{-4}$
II	771,0	0,1919	$3,846 \cdot 10^{-4}$
III	783,2	0,1889	$3,846 \cdot 10^{-4}$
IV	831,16	0,1780	$3,846 \cdot 10^{-4}$

Table 2.3: Dualsky nominal and experimental specification

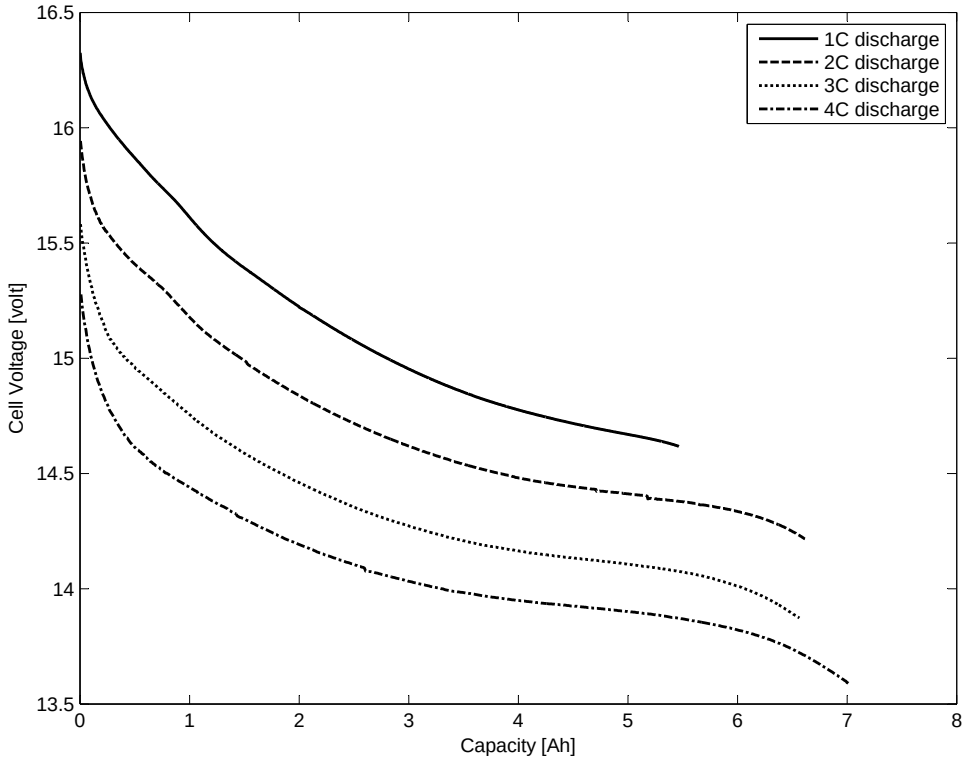

Figure 2.20: Voltage vs Capacity - Dualsky battery pack I

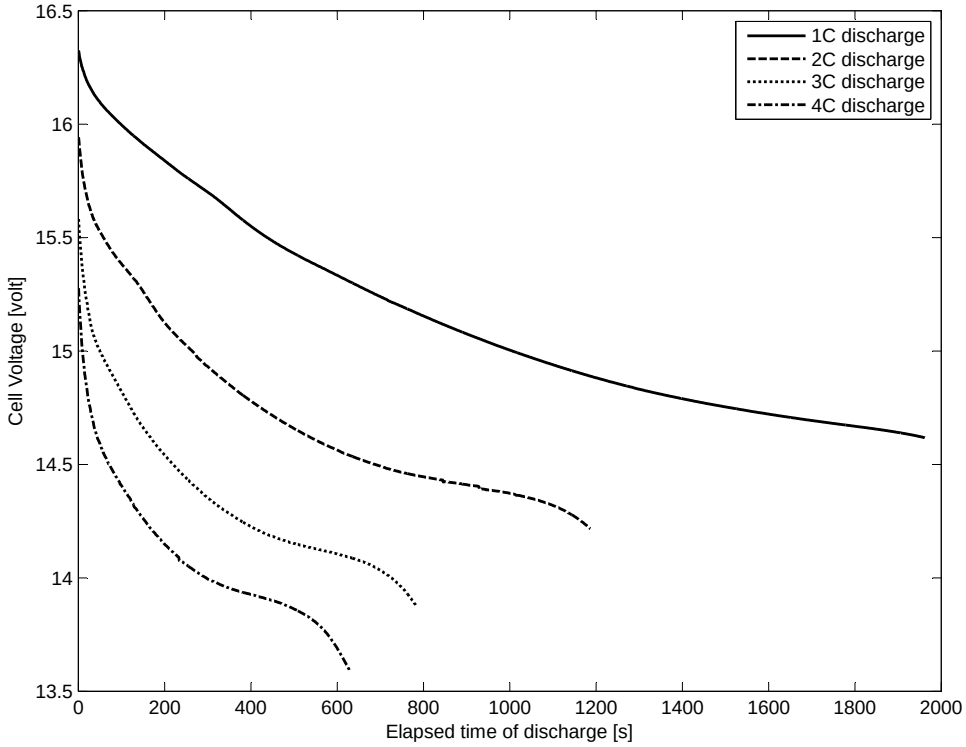

Figure 2.21: Voltage vs Elapsed time of discharge - Dualsky battery pack I

The discharge of the Li-Po cells show a linearly decreasing voltage as a function of residual capacity when discharged from the fully-charged voltage. So it is possible thinking the voltage constant during the discharge

The Peukert constant would be known for a particular battery type or established from experiment. So discharge curves are been analyzed to extract Peukert constant for each test. The average current in discharge was acquired during the test and substituted into equation 2.31:

$$k = \frac{ln\left(E/R_t\right)}{ln\left(C/[\bar{i}R_t]\right)} \tag{2.31}$$

where C is the rated capacity, E is the endurance in hours and $\bar{i}$ is the average current during the discharge and R_t is the rate of discharge ($\approx$ 1 Ah). For each of four battery pack, 4 discharge test are been performed and the Peukrt coefficient was calculated A summary of these results are presented in Tab.2.4

Peukert constant for the 4 Li-Po battery packs move inside a range of $1,12$ to $1,45$ in line with the average value of these kind of batteries.

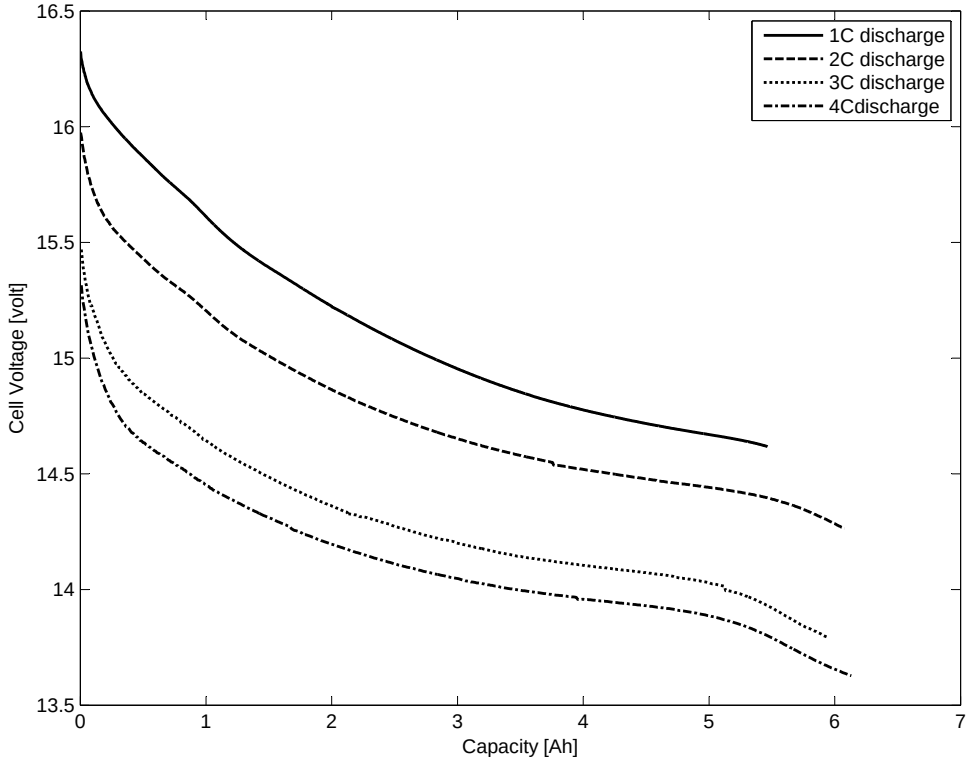

Figure 2.22: Voltage vs Capacity - Dualsky battery pack II

Pack	V_0	V_f	E	k
$[n^o]$	$[volt]$	$[volt]$	$[h]$	$[/]$
I	15,747	14,047	0,335	1,361
II	15,781	14,074	0,299	1,454
III	16,015	14,252	0,379	1,123
IV	16,063	14,318	0,361	1,293

Table 2.4: Average value acquired during discharge test

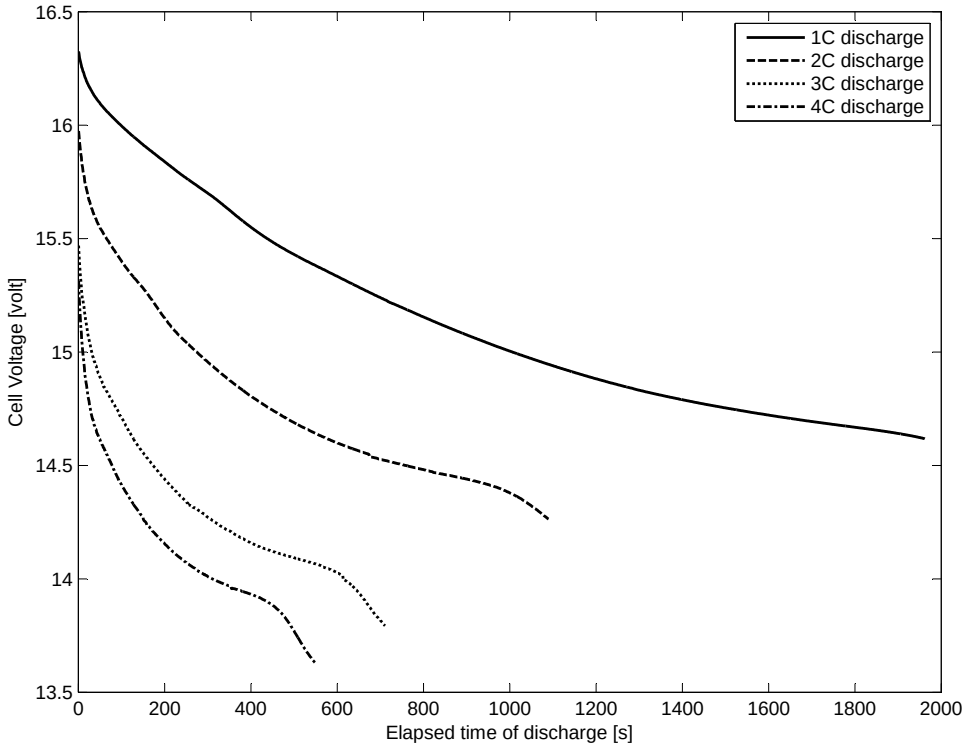

Figure 2.23: Voltage vs Elapsed time of discharge - Dualsky battery pack II

2.4 Main electronics/avionics systems

In modern multi-rotor, avionics is generally defined by 5 main components:

1. IMU : Inertial Measuring Unit
2. MC : Main Controller
3. PMU : Power Management Unit
4. GPS : GPS receiver antenna
5. Led : Led unit for visual warning and settings

MC is the component that is adopt to menage ESCs and payload (i.e. a gimbal)and other commands from traditional radio controller (pitch, roll, yaw, throttle, ...). IMU, that acquires accelerations for attitude determination, in many cases, it can be integrated inside the MC. MC is also connected to the LED and the PCU. PCU is connected to the power supply, for voltage detection and alarming, and to the GPS. Led unit allow the the ground pilot visual information to the connection status of the GPS and other warning. It is also

present a micro-usb port for parameter configuration and firmware upgrade. Fig.2.24 shows the typical avionics implementation on a multi-rotor platform with DJI NAZA system.

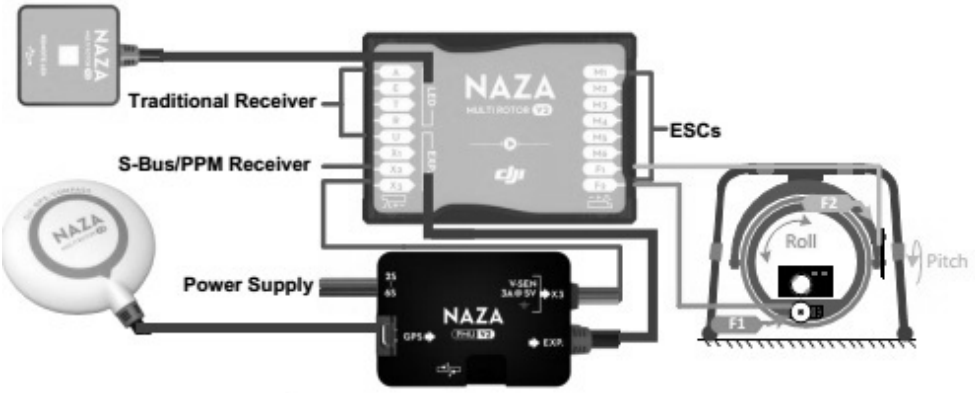

Figure 2.24: General scheme of multi-rotor avionics (i.e. DJI NAZA)

Three manufacturers, that allow available data to costumers, are been take into account. Manufacturers (i.e. DJI) have datasheets about main physical characteristics as volume and weight. Fig.2.25 shows the trend line about the mass in function of the volume.

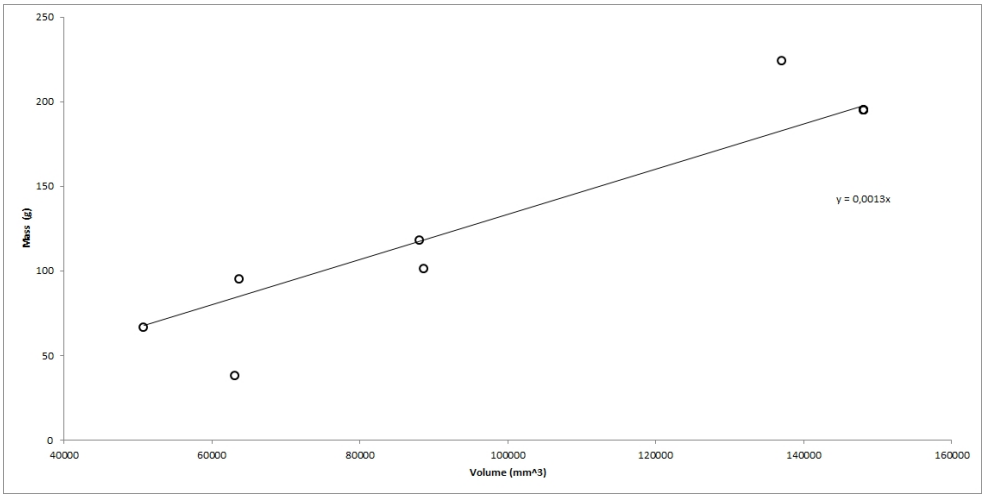

Figure 2.25: Avionics volume vs mass

The avionics trend line can be defined by a linear equation as:

$$Avio_{mass} = 0.0013 \cdot Avio_{vol} \tag{2.32}$$

Main average data are listed in Tab.(2.5):

http://www.dji.com/

Electronic / Avionics Average Data		
Total Volume	$108415,514$	$[mm^3]$
Total Weight	$142,43$	$[g]$
Max Power Consumption	$4,3$	$[Watt]$

Table 2.5: Multirotor average data

Inside Tab.2.6 it is shown the average value for the single element. In this case, in relation to the costumer choices, it is possible use equation 2.32 to find the estimate value of the avionics mass.

Single avionics components average data		
Component	$[g]$	$[mm^3]$
Flight Control	79	$49958,158$
GPS & Compass	$32,71$	$31560,911$
LED-BTU-I	$16,66$	$2937,833$
PMU	24	$8853,318$
IMU	70	$34461,203$

Table 2.6: Avionics components average weight & volume

2.5 Payload

A multi-rotor platform can fly with several type of payload: from electro-optical payload to atmospheric sensors. Multi-rotor is a very stable platform in hovering condition, and this allow the use especially with digital camera in different spectral range. Generally the camera is housed inside a particular robotic arm called Aerial Gimbals as shows in Fig.2.26 and Fig.2.27. Gimbals' duty is to stabilize the camera to a fixed attitude, generally parallel to the ground.

Gimbals take power directly to the main source of the platform and influence with this and with its weight the endurance performance. Obviously also the sensors or, in some cases, the camera, absorb power if there is not present a separate power source. Tab.2.7 list main parameters for payload as weight and power required useful for the performance and preliminary design calculations derived by DJI website.

Payload trade, related to Tab.2.7, can be plotted in Fig.2.29 to draw the trend line of equation 2.33.

Figure 2.26: Zenmuse Gimbals (DJI)

Figure 2.27: Zenmuse H4-3D (DJI)

Aerial Gimbals [*type*]	W Gimb. [kg]	Sugg. Camera [*type*]	W Camera [kg]	W payload [kg]
Zenmuse Z-15	1.3	$PanasonicGH2 + opt$	0.6	1.9
Zenmuse Z-15 GH3	1.22	$PanasonicGH3 + opt$	0.6	1.82
Zenmuse Z-15 GH4	1.26	$PanasonicGH4 + opt$	0.7	1.96
Zenmuse Z-15 5D	1.26	Canon eos 5D markIII	1.23	2.65
Zenmuse Z-15-5D III HD	1.53	Canon eos 5D markIII	1.23	2.76
Zenmuse Z15-BMPCC	11.26	nd	1.23	2.26
Zenmuse H3-2D		GoPro		0.23
Zenmuse H3-3D		GoPro		0.168

Table 2.7: Payload data from DJI

$$W_0 = 0,8895 \cdot W_{pay} + 10,71 \tag{2.33}$$

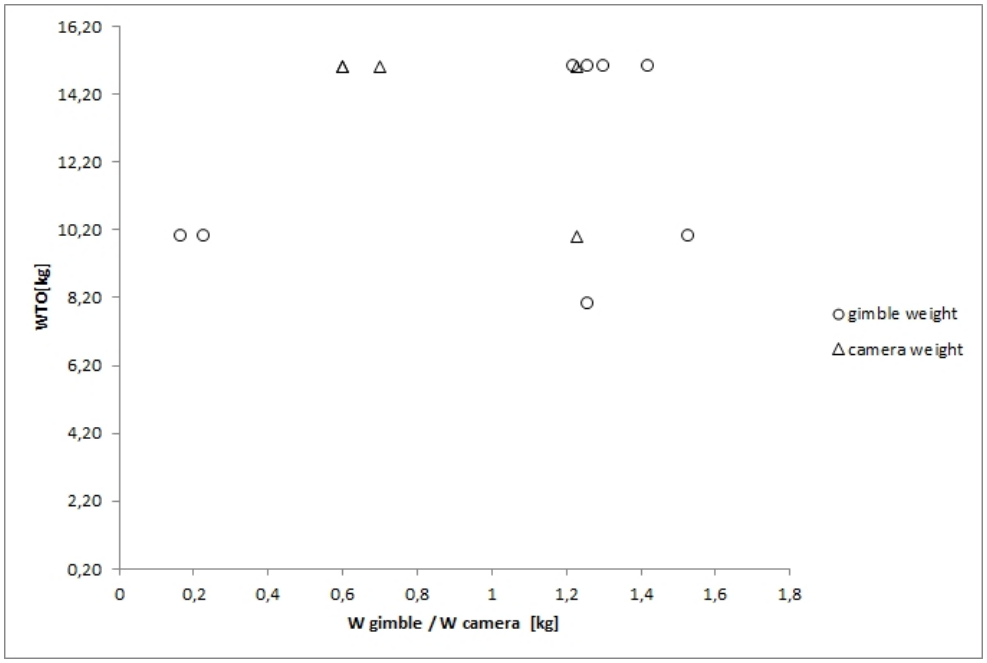

Figure 2.28: $W_{gimbals}$ & W_{camera} vs W_0 $[DJI]$

Collecting available information of commercial multi-rotor it is possible rewrite the equation of payload trade as 2.34 of Fig.2.30.

$$W_0 = 1,7691 \cdot W_{pay} + 1,5311 \tag{2.34}$$

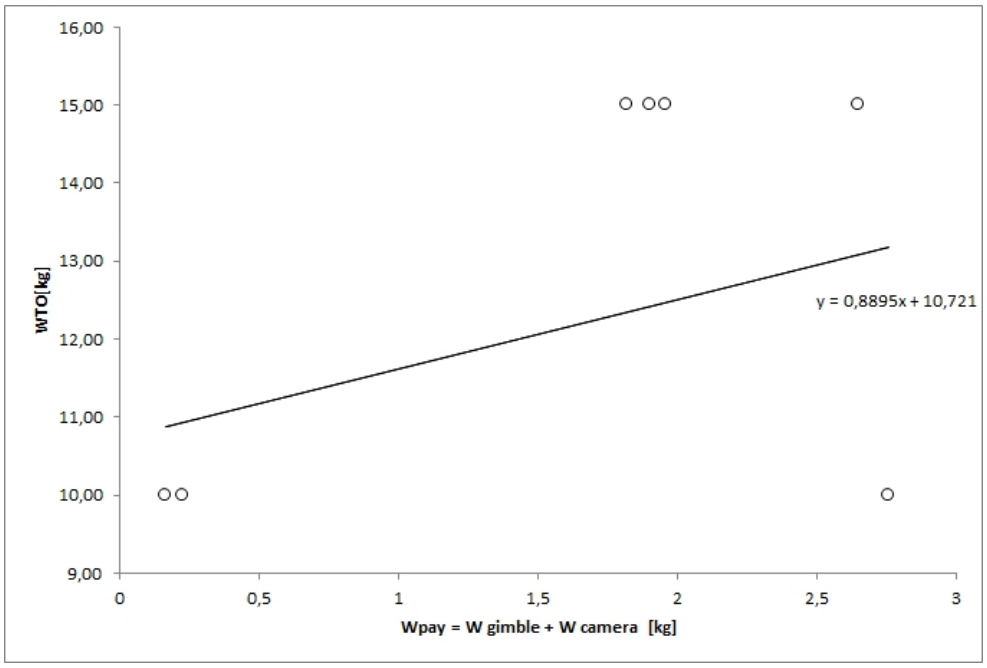

Figure 2.29: W_{pay} vs W_0 $[DJI]$

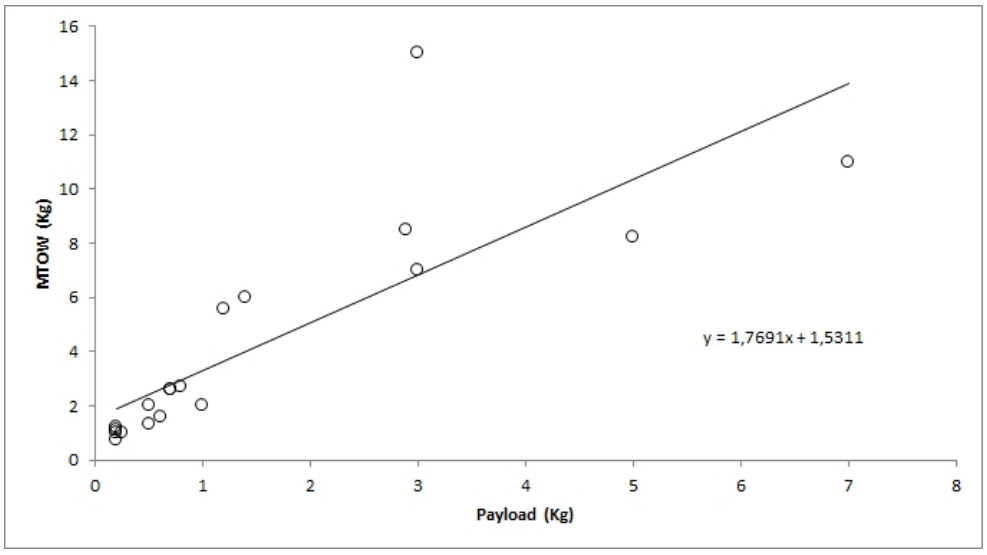

Figure 2.30: W_{pay} vs W_0 coomercial database

CHAPTER 3

Preliminary Design Methodology

The following paragraphs show how the classical methodology, used for airplane design, can be adopted for the new type of aerial platforms. in this case the methodology it has been applied on multi-rotor configuration powered by electrical DC motors.

In according to preliminary aircraft design methodology it is necessary to find relation between specific characteristics of commercial parts in order to get some mathematical equations. So for every type of platform it is possible define groups weight and statistical equations based on historical data of existing vehicles. So it is important create appropriate database in relation to the configuration and technologies in use.

3.1 Requirements and Constraints

The problem of endurance for any type of vehicles start approaching the power balance between the power required and the power available on board. Generally the vehicle power required depends to aerodynamic characteristic and by the weight of the platform. The designer find his first barrier against a free design by the National Rules defined to generate a little beat of order inside a more and more heterogeneous family of RPASs especially in civil fields. Aeronautical Rules divide vehicle in function its maximum take off weight. Regulation (EC) No 216/2008 mandates EASA agency to regulate UAS and in particular RPAS, when used for civil applications and with an operating mass of 150 Kg or more. Also

https://www.easa.europa.eu/unmanned-aircraft-systems-uas-and-remotely-piloted-aircraft-systems-rpas

EASA is member of JARUS which is currently developing recommended requirements for:

1. Licensing of remote pilots;
2. RPAS operations in VLOS and BVLOS;
3. Civil RPAS operators and Approved Training Organisations for remote pilots (JARUS-ORG);
4. CS-LURS and CS-LUAS below 600 Kg;
5. Performance requirements for 'detect and avoid' to maintain the risk of mid-aid collision below a TLS and taking into account all actors in the total aviation system;
6. Performance requirements for command and control data link, whether in direct RLOS or BRLOS and in the latter case supported by COM SP;
7. Safety objectives for airworthiness of RPAS ('1309') to minimize the risk of injuries to people on the ground;
8. Processes for airworthiness.

In our case, for a muti-rotor platform, the maximum take off weight is less than 150 kg. So national rules are in charge. ENAC principally divided RPASs into two main categories: one below 25 kg and one up 25 kg. Main difference between the two is that the platform up 25 kg follow the same rules and certification of a normal aircraft while below is the operator that is in charge for the certification and for the mission risk analysis.

If rules put on evidence requirements about flight time (endurance) and maximum take-off weight, for these vehicles, constraints are derived from scenario of operation and from payload. For example, if the platform have to be used in indoor condition, the frame dimension should be reduced and the disc propeller ducted in function to preserve propeller to possible collisions. Type of payload and its dimension constraints the frame and the relative Gimbals.

In relation of this the if the endurance is calculated in function of the maximum take off weight it will not be the optimum endurance but it will be a compromise in function of the weight requirement. For example the necessity to store or carry-on payload will increase the MTOW and will reduce endurance. The section of the endurance analytical solution is studied without any weight limitation (weight is still a variable).

https://http://jarus-rpas.org/

$https://www.enac.gov.it/La_Normativa_Enac/Regolamenti/Regolamenti_ad_hoc/info-122671512.html$

3.2 Take-Off Weight Buildup

According to the classical methodology for aircraft sizing [9], the design take-off gross weight, the critical term for every flight machine, is given by the total weight of the aircraft at the beginning of the mission that can be expressed as the sum of the all weights on the RPS at the takeoff condition:

$$W_0 = \sum_{i=0}^{max} W_i \tag{3.1}$$

For an electrically powered flying platform the take-off gross weight (W_0) it remains constant along the mission, and may be written as:

$$W_0 = W_e + W_{pp} + W_{el_{sys}} + W_b + W_p \tag{3.2}$$

where: W_0 is the takeoff gross weight, W_e is the empty weight (i.e. airframe weight without any system add), $W_{pp}$is the powerplant weight (i.e. DC motors total weight), $W_{el_{sys}}$ is the electronic systems weight (i.e. avionics, D/L and ESC systems), W_b is the battery weight, W_p is the payload weight (i.e.optical device, etc.).

W_{sys}, as defined, is the weight of the avionics and other system use inside the platform to perform the mission. Generally, for a multy-rotor platform, it is composed by a IMU, GPS, MC, LED and a PCU. The electronic systems weight can be defined as the sum of the avionics and the ESC as:

$$W_{el_{sys}} = W_{avion} + W_{esc} \tag{3.3}$$

It is important underline that the ESC system works like a servo for the rpm settings of the motor. If we consider an other type of platform the servo's weight have been take into account inside the list of partial weights.

Solving equation 3.2, the estimation of W_0 can be defined as:

$$W_0 = \frac{W_{pp} + W_{el_{sys}} + W_b + W_p}{1 - \frac{W_e}{W_0}} \tag{3.4}$$

Equation 3.4 shows that the elements of the numerator are not variable during the iteration and the denominator is defined by the only empty weight fraction because is not present the fuel fraction. This put on evidence that electric vehicles do not change their weight during the flight mission.

3.2.1 Commercial Multirotor analysis and Empty-Weight Estimation

First step in take-off weight buildup is the empty weight fraction, W_e/W_0, estimation. While in commercial aircraft design, due to the large amount of data available in the literature, a first guess of W_e/W_0 does not represent a critical issue, on the contrary, for multi-rotors, since the design of multi-rotors aircraft is relatively new (and mostly based on the scale-model aircraft enthusiastic experience on rotary wings models), the empty weight fraction estimation may be affected by a poor availability of data.

For the purposes of the present work, seven international multi-rotors manufacturers data available have been taken into account for collecting platform weight features. Among them, Microdrones and Dragan-Flyer provide technical information about multi-rotors performance for customers.

On the basis of (even limited) data available a first database showing platform geometry, mass features, and flight performance is made, providing suitable values that can be used as a first guess for multi-rotors preliminary design. Four and six rotors configurations (namely quadcopters and hexacopters, respectively) have been taken into account to list the database. All these type of multirotors are built of composite material for frame, landing gear and brackets and only in small proportion aluminium parts to build stiffeners. Composite material allow to reduce empty weight.

The empty weight fraction, W_e/W_0, is statistically estimated from historical trends obtained from the available literature. It results to vary from 0.9 to 0.3, and it decreases while the total weight of the platform is increasing. It is worth noticing that the number of rotor does not seem to have a direct influence on total weight. The Microdrone md4-1000 (quad-copter) and DJI S800 (hexa-copter) present the same total weight but a different configuration.

Fig. 3.1 shows the empty weight trends obtained by available literature. The trend line is defined by the following linear expression:

$$\frac{W_e}{W_0} = -0,00118 \cdot W_0 + 0,6613 \tag{3.5}$$

3.2.2 Determination of the battery mass

The specific energy of the battery can be defined in function of the power requirement and the flight time [20] as:

http://www.microdrones.com/
http://www.draganfly.com/

Dragan Flyer X4-P		
Width	0,87	[m]
Lenght	0,87	[m]
Top Diameter	1,06	[m]
Height	0,32	[m]
Helicopter Weight	0,68	[Kg]
Payload	0,25	[Kg]
MTOW	0,98	[Kg]
Max Climb/Desc. Rate	2	$[m/s]$
Max Turn Rate	90	$[deg/sec]$
Max Air Speed	50	$[Km/h]$
Max Altitude (ASL)	2430	[m]
Engine	4	[num.]
Engine Type	DC Brushless	
Battery Type	LiPo	
Battery Capacity	5400	$[mAh]$
Battery Voltage	14,8	[v]

Table 3.1: Example of Commercial Multirotor Data available

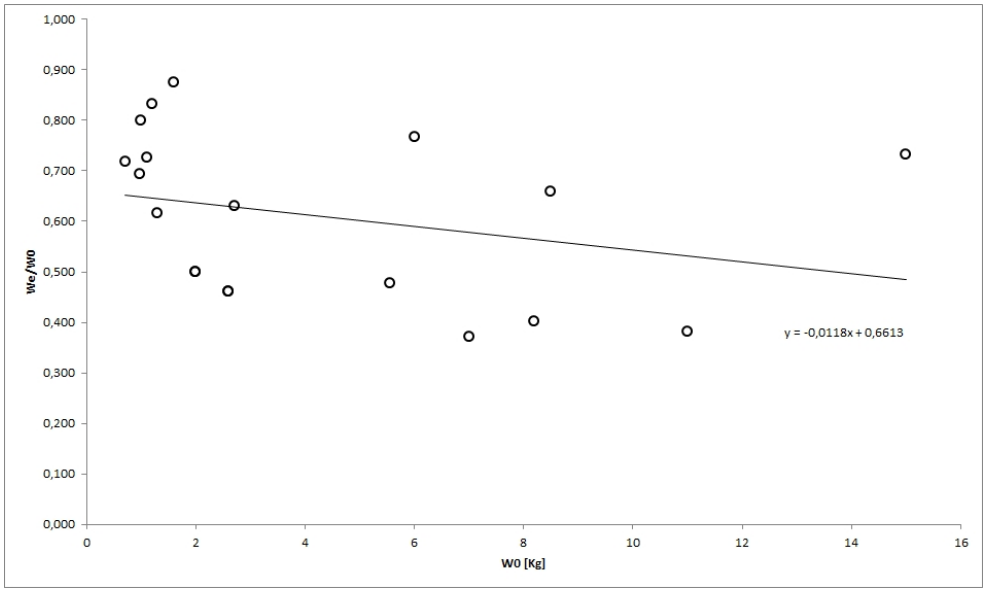

Figure 3.1: Empty Weight fraction Trend

$$E_b = \frac{FT \cdot Power\ req.}{f_{DOD} \cdot \eta_{discharge}} \tag{3.6}$$

where:

- $f_{DOD} \cong 0.8$
- $\eta_{discharge} \cong 0.95$

And the product of flight time and power requirements can be separated into the several mission segments as:

$$\begin{aligned} FT \cdot Power\ req. = &(FT_{tot} \cdot P_{sys}) + \\ &+ (FT_{climb} \cdot P_{climb}) + \\ &+ (FT_{cruise} \cdot P_{cruise}) + \\ &+ (FT_{loiter} \cdot P_{hover}) \end{aligned} \tag{3.7}$$

Once the E_b has been found, the mass of the battery is determined through equation ($E_b = 137,93 m_b$) or graphically.

3.2.3 Rotorcraft Power Requirements

For rotorcrafts, the power requirements are given by the analysis of Momentum Theory (MT) and Blade Element Theory (BET). For vertical climb and hover (setting climb rate to 0) the power [9] is given by:

$$P_{climb} = \frac{1}{\eta_p \eta_{el} \eta_{mecc}} \left[\left(\frac{fW}{FM} \sqrt{\frac{fW/S}{2\rho}} \right) + \frac{WV_{climb}}{2} \right] \tag{3.8}$$

Where: W is the RPAS weight (in this case multi-rotor weight), S is the total rotor disck area, FM is figure of merit (generally with a value of $0.4 \div 0.8$ in relation to the type/dimension of the propeller blade), V_{climb} is the climb rate (= 0 for hover), f is the downwash on fuselage (≈ 1.03).

For climbing forward flight and level forward flight (setting $\gamma = 0$) the power required is given by:

$$P_{forclimb} = \frac{V}{\eta_p \eta_{el} \eta_{mecc}} \left[q \left(\frac{D}{q} \right) + \frac{W^2}{4eqS} + W \cdot sin\left(\gamma\right) \right] \tag{3.9}$$

Where: η_p is the propeller efficiency ($0.4 \div 0.5$), η_{mecc} is the mechanical efficiency ($1 \div 0.9$), η_{el} is the electrical efficiency (≈ 0.9), γ is the climb path angle.

Generally multirotors propellers are directly driven by the DC motor. The η_{mecc} in this case is equal to 1; but if we consider the possibility to use commercial variable pitch propeller for new multirotor configuration, we have to take into account a value different to 1. The $\left(\frac{D}{q}\right)$ ratio is the drag area of the fuselage and could be analyzed as shape factors and skin friction value.

3.2.4 Analysis and Results

Now with the methodology described in this thesis, an example of preliminary calculation can be made. Generally multi-rotor RPV has mission profile like Military Radius Mission, but the missions prefer are surveillance and border control to icrease security and provide observation capabilities. For example multi-rotor can rise to heights in few seconds and take and transmit with appropriate payload and data-link image from its payload (i.e. CCD/IR cameras, cellular antennas, hyperspectral sensors, ...)

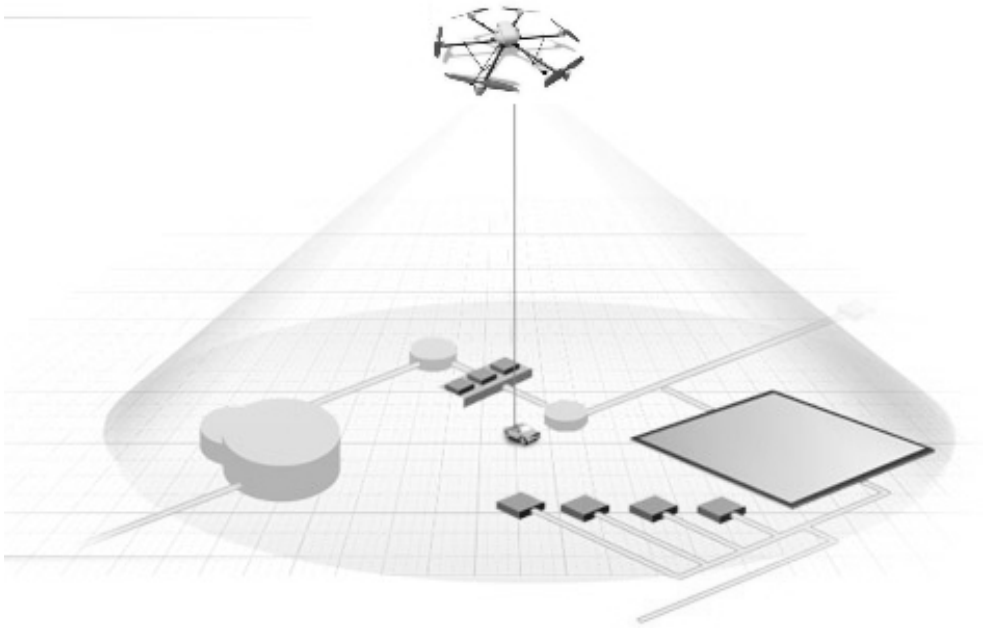

Figure 3.2: Multi-rotor Hovering Observation Mission

It is considered the case of a hexa-rotors RPV. The statistical data used in the analysis are the following:

Average Value from Manufacturers Data Weight, Dimension & Payload		
Multirotor W_e	1,889	$[Kg]$
Payload	0,9558	$[Kg]$
MTOW	3,156	$[Kg]$
$\frac{W_e}{W_0}$	0,627	[]
Propeller Diameter (D)	260	$[mm]$
Performance		
FlightTime	38	$[min]$
Radius in RC	500	$[m]$
Radius in WP	4000	$[m]$

Table 3.2: Average Values from Manufacturers

Now define a mission of 15 minutes of hovering over a specific point with a payload of 0.5 Kg. This is a possible mission for a surveillance multi-rotor that departs from ground and climb on a fixed operating altitude, see Fig.3.2. The payload could be any optical/IR devices. It is assumes also the air density (ρ) at sea level.

The following values, listed in Tab.3.3, are assumed for the various coefficients.

M	0,6	
f	1,3	
η_p	0,4	
η_{el}	0,9	
η_{mecc}	1	(direct drive)
f_{DOD}	0,8	
$\eta_{discharge}$	0,95	
ρ	1,225	$[Kg/m^2]$

Table 3.3: Aeromechanical Coefficients

In relation to the mission segment, in this case a 15 min of hovering, the calculation starts from a $W_{0_{guess}}$ of 4 Kg. The first step is to calculate the power need to perform the mission using equation3.8 and equation 3.6. The power need, in relation to the flight time, allow to find the battery and motor mass. In our case:

P_{hover}	E_b	W_{batt}	$W_{DC_{motor}}$
$[W]$	$[W\dot{h}]$	$[Kg]$	$[Kg]$
$921,549$	$303,141$	$2,198$	$0,037$

Table 3.4: Power need, battery & motor characteristics

Power and motor mass allow to find an adequate DC engine inside the database. Scorpion $HKII-2212-12$ fits the results.

Scorpion $HKII-2212-12$		
Kv	Max Current	$W_{DC_{motor}}$
$[rpm/volt]$	$[A]$	$[Kg]$
2580	38	$0,038$

Table 3.5: Scorpion DC engine char.

After choice the DC motor it can be define the electronic speed control (ESC) using the maximum motor current incremented of 20%. In the same manner of the DC motor choice, using equation (2.18) and ESC database we can find the right elements: Turnigy Multistar 45 Amp using equation (2.17) and (2.18).

Turnigy Multistar 45 Amp		
Max Current	Max Current +20%	$W_{DC_{motor}}$
$[A]$	$[A]$	$[Kg]$
38	$45,6$	$0,044$

Table 3.6: ESC char.

For avionics components, they are take into account a complete suite (IMU, PCU, ...) with an average weight of $0,142$ kg.

These results are the input for the iterative calculation.To find iteratively the takeoff gross weight, a guess value of it is fixed, generally close to the main historical value, and used as one shot in the dark inside the equation 3.4. If the result value does not match the guess value, the result value is used as next guess value. Just few iterations will cover the result. This first-order sizing process is shown in Tab.3.7.

The results of the preliminary calculation are shown into Tab.(3.8).

http://www.scorpionsystem.com/
http://www.turnigy.com/

W_0	$\frac{W_e}{W_0}$	$W_{0_{calc}}$	W_e
$[Kg]$	[]	$[Kg]$	$[Kg]$
4,000	0,611	8,567	5,232
8,567	0,588	6,553	3,855
6,553	0,598	6,714	3,016
6,714	0,597	6,701	4,003
6,701	0,597	6,702	4,004
6,702	0,597	6,480	4,004
6,702	0,597	6,480	4,004

Table 3.7: Results of the iterative calculation

Summary of preliminary design results		
RPV Configuration	Hexa-rotor	
W_0	$6,702$	$[kg]$
W_e	$4,004$	$[kg]$
$DCmotor$	Scorpion HKII$-2212-12$	
$W_{DC_{TOT}}$	$0,230$	$[kg]$
ESC	Turnigy Multistar 45 Amp	
$W_{ESC_{TOT}}$	$0,265$	$[kg]$
W_{batt}	$2,198$	$[kg]$
W_{pay}	$0,5$	$[kg]$
W_{avion}	$0,142$	$[kg]$

Table 3.8: Preliminary design results

By the way it is possible to check also the trend of the empty weight in function of the disk loading.

n	D	S	W_0	W_e	T/S
$[n_{rot.}]$	$[m]$	$[m^2]$	$[Kg]$	$[Kg]$	$[Kg/m^2]$
6	0,38	0,6801	6,480	4,004	9,856
6	0,36	0,6104	6,746	4,162	11,444
6	0,34	0,5445	7,041	4,336	12,404
6	0,32	0,4823	7,370	4,529	15,849
6	0,30	0,4239	7,741	4,744	18,979
6	0,28	0,3693	8,161	4,987	22,954

Table 3.9: Disk Loading versus W_e

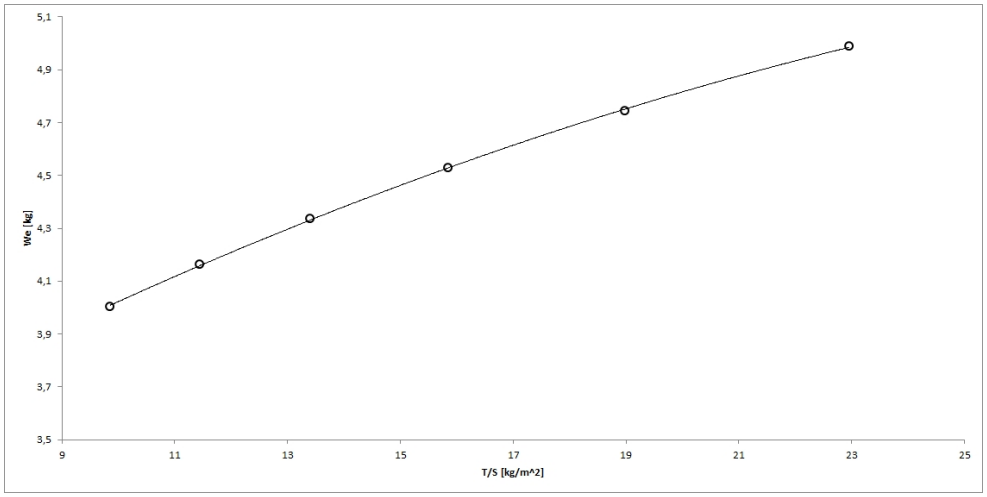

Figure 3.3: Disk Loading versus Empty Weight

As shown in Tab.3.9 and in Fig.3.3 to an increase of Disk Loading corresponds an increase of W_e. Obviously it is not possible reduce drastically the total Disk Surface area but this puts on evidence that is possible design compact multirotor with low empty weight [19].

CHAPTER 4

Best Endurance Condition

Endurance, for electrical vehicle, is directly connected to the battery capacity and technology. Nowadays, multi-rotor platform do not have again a relevant endurance for which it is possible use these kind of machine till more than 15-20 minutes. Some industrial project as IAI ETOP, acronym of Electric Tethered Observation Platform (Fig.4.1), have completely removed the endurance problem build a umbilical cable that supply without limit the platform; in this case the platform can carry-on a payload of more than 20 Kg.

At the moment previous studies are developed for endurance of fixed wing platform ([6], [4], [5]) but nothing for helicopter or multi-rotor. The following chapter explain the the theoric dissertation about multi-rotor endurance and the validation through the use of a test banch and several flight test with a commercial platform.

4.1 The endurance for electrical RPAS

How it is been explained in the previous chapter about the weight fraction, it is possible rewrite equation 3.2 in a more usefull expression to use to calculate endurance. Let us consider a rotary-wing platform equipped with a payload for a specific mission. The total take-off weight can be expressed as:

$$W_{to} = W_{eo} + W_p + W_b \tag{4.1}$$

http://www.iai.co.il/2013/35735-41817-en/IAI.aspx

Figure 4.1: IAI ETOP

where W_{eo} is the empty-operative weight that includes the a) frame weight (structure and rigging), b) the driving system weight (motors, regulators, and propellers), and c) the avionics weight (autopilot and telemetry), W_p is the payload weight, and W_b is the battery weight.

For the purposes of the present analysis, the total power required for flight is

$$P_r = P_h + P_{ap} \tag{4.2}$$

where P_h is the power required for the hovering condition and P_{ap} is the power required for avionics and payload. For rotary-wing aircraft, the power required in hovering condition is given by [11]

$$P_h = \frac{W_{to}^{3/2}}{f\sqrt{2\,\rho\,A_t}} \tag{4.3}$$

where f is the figure of merit of the rotor, ρ is air density, and A_t is the total disc area. After naming $\lambda = \sqrt{2\,\rho\,A_t}$, by imposing the balance between the required and available power from the battery, the current draw, i, for the hovering condition is given by:

$$i = \frac{P_r}{\mathcal{V}} = \frac{1}{\mathcal{V}}\left(\frac{W_{to}^{3/2}}{\lambda\,f} + P_{ap}\right) \tag{4.4}$$

where $\mathcal{V}$ is the battery voltage that, in general, is a function of both current draw and capacity. From the definition of the discharge ratio, $dC/dt = i$, it is straightforward to obtain the specific endurance

$$\frac{dt}{dC} = \frac{\mathcal{V}\,\lambda\,f}{W_{to}^{3/2} + P_{ap}\,\lambda\,f} \tag{4.5}$$

For a nominal battery capacity C_0, the actual available capacity C at the discharge rate i is provided by the Peukert equation, [12],

$$C = C_0\left(\frac{C_0}{i\,t_0}\right)^{k-1} \tag{4.6}$$

where t_0 is the rated discharge time, and k is Peukert's coefficient. By considering the complete discharge of the available capacity, flight endurance is given by the following integral:

$$t = \int_0^C \frac{\mathcal{V}\,\lambda\,f}{W_{to}^{3/2} + P_{ap}\,\lambda\,f}\,dC \tag{4.7}$$

4.1.1 Constant Battery Voltage during the discharge

The battery voltage is supposed to be constant during the discharge [6, 14]. As a matter of fact, for constant power applications, Li-Po cells show a linearly decreasing voltage

as a function of residual capacity (with a negligible dependency on current draw) when discharged from the fully-charged voltage, $\mathcal{V}_f$, to the standard voltage, $\mathcal{V}_0$.

Let η express the fraction of the nominal capacity where the discharge process shows a linear behaviour. The available capacity becomes

$$C = \eta\, C_0 \left(\frac{\eta\, C_0}{i\, t_0}\right)^{k-1} \tag{4.8}$$

By imposing in Eq.4.7 the discharge at the equivalent constant voltage, $\mathcal{V}_e = (\mathcal{V}_f + \mathcal{V}_0)/2$, the endurance turns to

$$t = \frac{\mathcal{V}_e\, \lambda\, f}{W_{to}^{3/2} + P_{ap}\, \lambda\, f} \int_0^C dC = \frac{\mathcal{V}_e\, \lambda\, f}{W_{to}^{3/2} + P_{ap}\, \lambda\, f}\, \eta\, C_0 \left(\eta\, \frac{C_0}{i\, t_0}\right)^{k-1} \tag{4.9}$$

4.1.2 Definition of the Figure of Merit

The Figure of Merit, first introduced by Renard (1903) and Glauert (1935), with the power loading (T/W), is one of the parameter that define the efficiency of one rotor. Anyway it is of difficult definition because, involved inside its, many parameters as solidity, blade aspect ratio, ecc. This quantity is equivalent to a static thrust efficiency and defined as the ratio to the ideal power required to hover to the actual power required, that is:

$$\frac{P_{ideal}}{P_{meas}} = \frac{{C_T}^3/2}{\sqrt{2}C_P} < 1 \tag{4.10}$$

Where the measured value of the power coefficient, C_P, will include induced and non ideal physical effects that have origin from viscosity. For an helicopter rotor a value of 0.7 and 0.8 represent a good hovering performance for a generic rotor with conventional technology Fig.4.2.

Instead, propeller used for little RPAS, have an efficiency from a peak of 0.65 to near 0.28 (very poor propeller)[21], thus indicate that proper propeller selection have a dramatic effect on vehicle performance. To investigate endurance it is necessary to know the FM value.

4.1.3 Thrust and Power Measurement

The value of the Figure of Merit is obtained using a custom test bench. The value of thrust is acquired by a load cell model Deltatech $S - AL - A/25kg$. The power required is measured via APM Power Module current/voltage sensor and all the signals is acquired

http://www.deltatechitaly.com
http://store.3drobotics.com/products/apm-power-module-with-xt60-connectors

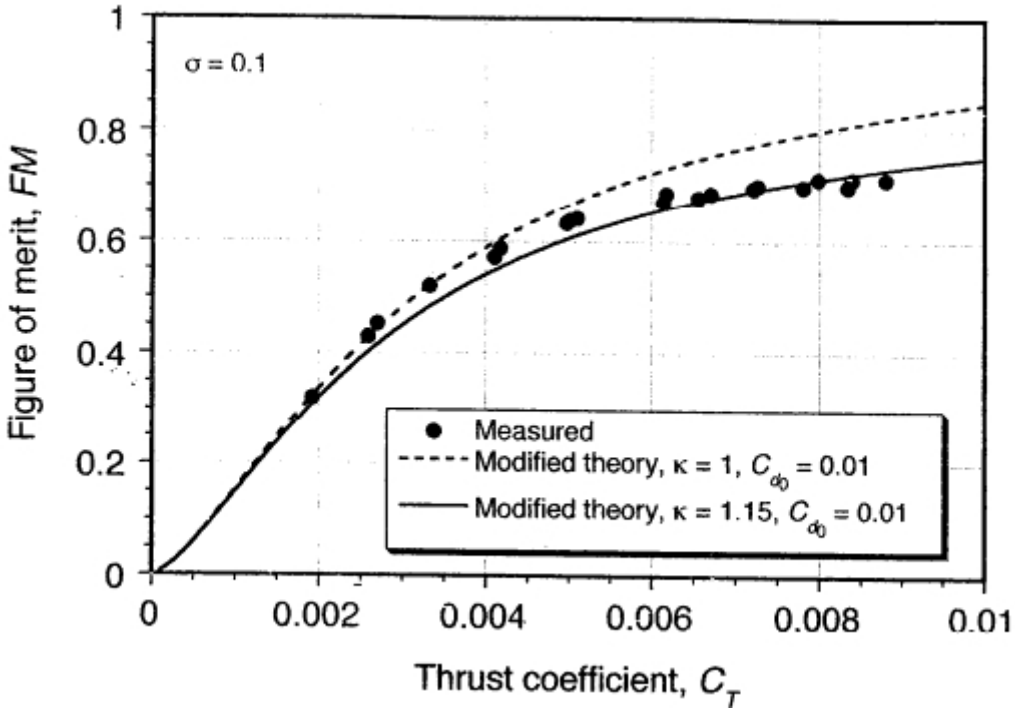

Figure 4.2: Figure of Merit prediction made with modified momentum theory [11]

and elaborated through a micro-controller Arduino 2. For the test is used a Dji DC motor model 2212/920KV with a 10x45 propeller driven by a 30A ESC.

Starting from 30% to 85% of throttle, steps of 5%, five acquisitions are done for any steps. Two battery pack of Li-Po battery ($4S - 10.000$ mAh) linked in parallel provide the power for the whole system The time for the test is about 10 sec and the packs are recharged after any test. This procedure is necessary to ensure a system voltage constant and a basic time to permit at the engine to reach the performance rate.

The propeller, a 10 inch diameter, was driven by an ESC system that control and mount on a DC out-runner motror. For any steps of throttle in % five value of thrust and power are been acquired and later elaborated to find the FM value as shows in Fig.4.4.

After acquisition, it is been calculated the mean value to trace the approximate trend of the figure of merit as show in Fig.4.5.

The data acquisition are needed to build a new model of FM useful for the endurance estimation.

http://arduino.cc/

Figure 4.3: Test Banch used for FM acquisition

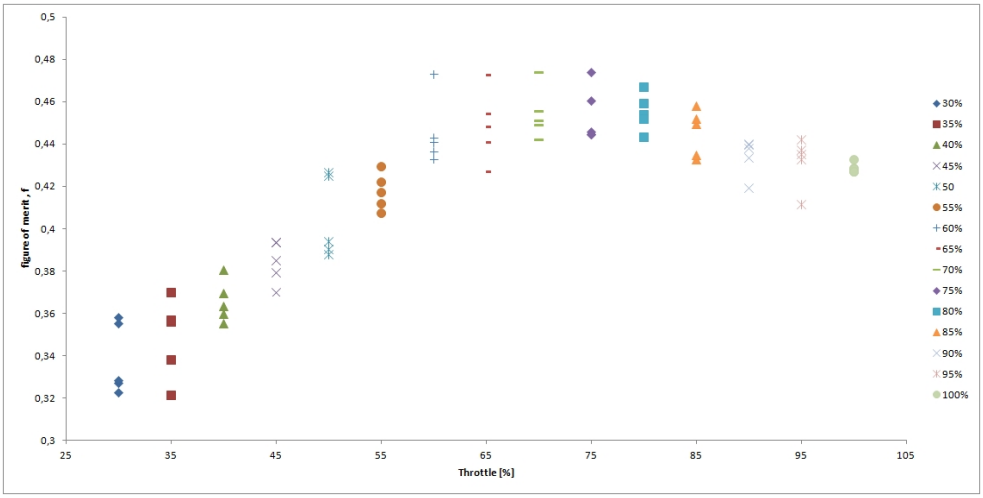

Figure 4.4: Experimental value of FM

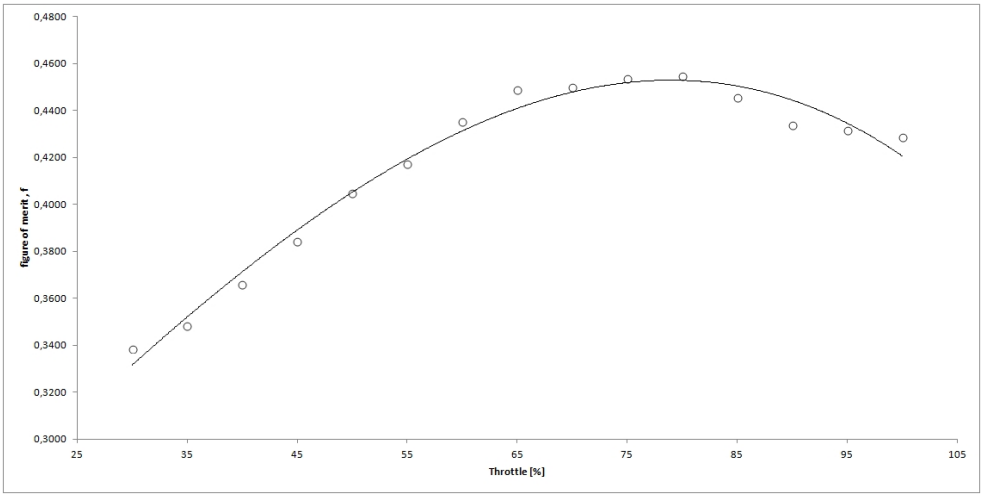

Figure 4.5: Experimental trend of FM

4.1.4 A new approximation of FM

Rotor figure of merit is supposed to be a slowly-varying power function of the rotor thrust. The following model is proposed:

$$f = f_0 \left(\frac{W_{to}}{T_0\, n} \right)^m \tag{4.11}$$

where T_0 is the rotor thrust at a reference percentage of throttle position (i.e. at 55%), and n is the number of rotors. Model parameters, f_0 and m, are obtained by available data from the manufacturer and/or by means of an experimental characterization.

Via experimental data the FM is plotted into the rage of thrust used, Fig.4.6, and the power trend line define the value of the coefficient.

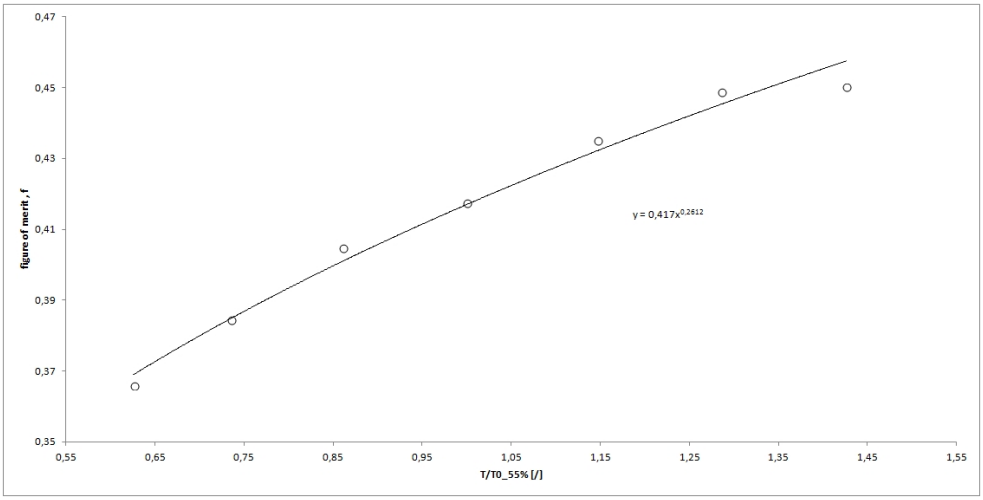

Figure 4.6: Rotor FM with a thrust value of $T_0 = 55\%$

4.1.5 Maximum endurance condition

Letting α indicate the battery weight/energy ratio, aircraft take-off weight can be expressed as

$$W_{to} = W_0 + W_b = W_0 + \alpha\, \mathcal{V}_e\, C_0 \tag{4.12}$$

where $W_0 = W_{eo} + W_p$ is the zero-capacity weight, representing the weight of the aircraft without the battery system. By substituting Eqs.4.4 and 4.11 into Eq.4.7, and by taking into account Eq.4.12, endurance in hovering flight is given by

$$t = t_0 \left[\frac{\mathcal{V}_e\, \eta\, f_0\, \lambda}{t_0\, (T_0\, n)^m} \right]^k \Phi(C_0) \tag{4.13}$$

where the function

$$\Phi(C_0) = C_0^k \left[(W_0 + C_0\,\mathcal{V}_e\,\alpha)^{m-3/2} + \frac{f_0\,\lambda}{(T_0\,n)^m}\,P_{ap} \right]^{-k} \tag{4.14}$$

depends on the nominal battery capacity.

Provided that all the parameters in the bracketed coefficient of Eq.4.13 are constant, the best endurance condition is obtained by taking the derivative of Φ with respect to C_0 and imposing $d\,\Phi(C_0)/d\,C_0 = 0$. The nominal capacity allowing for the maximum endurance is thus obtained by solving the equation

$$\frac{\mathcal{V}_e\,\alpha\,(2\,m-3)\;(W_0 + C_0\,\mathcal{V}_e\,\alpha)^{1/2}\;(T_0\,n)^m}{(W_0 + C_0\,\mathcal{V}_e\,\alpha)^{3/2}\;(T_0\,n)^m + P_{ap}\,f_0\,\lambda\;(W_0 + C_0\,\mathcal{V}_e\,\alpha)^m} + \frac{2}{C_0} = 0 \tag{4.15}$$

To the best of the authors' knowledge, an analytical solution to the problem cannot be found when $\Phi(C_0)$ assumes the form expressed in Eq.4.14. Nonetheless approximate closed-form solutions can be obtained on the basis of two different simplifying assumptions.

Case 1

The rotor figure of merit is assumed to be constant, $f \approx f_0$. This assumption holds when f shows negligible variations within the operational range of motor throttle (i.e $|m| \ll 1$), or when the aircraft is sized so that the driving system operates in the neighborhood of an assigned throttle position. By imposing $m = 0$ in Eq.4.15 the problem reduces to:

$$\frac{2}{C_0} - \frac{3\,\mathcal{V}_e\,\alpha\;(W_0 + C_0\,\mathcal{V}_e\,\alpha)^{1/2}}{(W_0 + C_0\,\mathcal{V}_e\,\alpha)^{3/2} + P_{ap}\,f_0\,\lambda} = 0 \tag{4.16}$$

By solving with respect C_0, the nominal capacity for the maximum endurance becomes

$$C_0|_{me}^{(1)} = \frac{1}{\mathcal{V}_e\,\alpha}\;(\Psi_0 - W_0) \tag{4.17}$$

provided

$$\Psi_0 = \frac{\left[\left(\sqrt{f_0^2\,\lambda^2\,P_{ap}^2 - W_0^3} + P_{ap}\,f_0\,\lambda \right)^{2/3} + W_0 \right]^2}{\left(\sqrt{f_0^2\,\lambda^2\,P_{ap}^2 - W_0^3} + P_{ap}\,f_0\,\lambda \right)^{2/3}} \tag{4.18}$$

The maximum value for hovering time is obtained by substituting Eq.4.17 into Eq.4.14, providing the following expression:

$$t|_{me}^{(1)} = t_0 \left[\frac{f_0\,\eta\,\lambda\;(\Psi_0 - W_0)}{t_0\,\alpha\,\left(\Psi_0^{3/2} + P_{ap}\,f_0\,\lambda \right)} \right]^k \tag{4.19}$$

Results obtained under the hypothesis of constant figure of merit are effective in all applications where the aircraft take-off weight is limited to a maximum value, $W_{to}^{\star}$, because

of mission and/or regulation constraints. As a matter of fact, for a given take-off weight, the platform figure of merit is fixed, making Eqs. 4.17 and 4.19 provide an accurate estimation of battery capacity and endurance. As a further contribution, by taking into account Eq. 4.12, it is straightforward to obtain from Eq.4.16 the following expression,

$$C_0|_{W_{to}^\star} = \frac{2}{3}\frac{W_{to}^{\star\,3/2} + P_{ap}\, f_0\, \lambda}{\alpha\, \mathcal{V}_e\, W_{to}^{\star\,1/2}} \tag{4.20}$$

which represents the nominal capacity for the maximum endurance in the presence of a constraint on the maximum take-off weight.

Case 2

The power required for systems and payload is neglected, $P_r \approx P_h$. This assumption is usually valid in the following three scenarios: 1) there is no power-consuming payload on board and aircraft systems only consist of autopilot and telemetry whose power consumption usually has a negligible effect on endurance, 2) the payload uses a dedicated battery system and the weight of such battery is already included in W_0, 3) the power required for avionics and payload is small if compared to the power required for the hovering condition, $P_{ap}/P_h \ll 1$. After imposing $P_{ap} = 0$ into Eq.4.15, the problem is thus reduced to

$$\frac{2}{C_0} + \frac{\mathcal{V}_e\, \alpha\, (2\, m - 3)}{W_0 + C_0\, \mathcal{V}_e\, \alpha} = 0, \tag{4.21}$$

which solution provides

$$C_0|_{me}^{(2)} = \frac{1}{\alpha\, \mathcal{V}_e}\frac{2\, W_0}{1 - 2\, m} \tag{4.22}$$

By substituting this latter result into Eq.4.14 one has

$$t|_{me}^{(2)} = t_0 \left[\frac{2\, f_0\, \eta\, \lambda}{t_0\, \alpha\, (1 - 2\, m)}\frac{W_0^{\,m-1/2}}{(T_0\, n)^m}\left(\frac{2\, m - 3}{2\, m - 1}\right)^{m-3/2}\right]^k \tag{4.23}$$

Optimal capacity and endurance estimation carried out with variable figure of merit represent a suitable solution for addressing the performance analysis with respect to battery capacity of already existing platforms. In particular, the endurance prediction shows an increased accuracy for a wide range of commercial multi-rotor platforms equipped with a stabilised photo/video payload for surveillance, aerial photography, and low-cost photogrammetry applications, where the ratio P_{ap}/P_h has the same order of magnitude of 10^{-2}. Table 4.1 shows P_{ap}/P_h and other design parameters values for a selection of platforms available on the market.

Although $C_0|_{me}^{(1)}$, and $C_0|_{me}^{(2)}$ represent acceptable approximations for a class of problems involving hovering flight endurance, there are cases where a further simplified result would be useful. As a matter of fact, in the preliminary phase of the design process, the selection

Platform	W_{to} [N]	W_p [N]	W_{eo}/W_{to}	W_b/W_0	P_{ap}/P_h	C_0 [Ah]	t [min]
DJI S1000	107.91	18.63	0.56	0.26	< 0.01	15	15
Altura ATX8	61.80	24.52	0.51	0.37	< 0.01	16.6	19
DJI S900	80.44	18.63	0.55	0.23	< 0.01	12	18
DJI S800 evo	68.67	18.63	0.52	0.21	< 0.01	15	20
Altura ATX4	51.99	9.81	0.41	0.66	< 0.01	16.6	35
DJI F550	22.56	2.25	0.51	0.35	0.023	5.4	13
HighOne Quad	76.51	12.75	0.58	0.34	< 0.01	16	16
tarot t810	66.70	14.71	0.51	0.36	< 0.01	11.6	14
E1100-V2	83.38	13.73	0.65	0.22	< 0.01	12	11
Aibot-X6	65.23	19.62	0.51	0.23	< 0.01	10	12

Table 4.1: Relevant parameters of a selection of existing platforms

and/or characterisation of the driving system is still an occurring problem. Thus, a simpler solution, describing the best endurance condition without the need of detailed information on rotor features, may represent a valuable starting guess for the aircraft take-off weight estimation. By imposing $m = 0$ into Eq.4.22 one gets

$$C_0|_{me}^{(0)} = \frac{1}{\alpha\,\mathcal{V}_e}\,(2\,W_0) \tag{4.24}$$

and

$$t|_{me}^{(0)} = t_0\,\left[\frac{2\,f_0\,\eta\,\lambda}{3\,\sqrt{3}\,\alpha\,t_0}\,W_0^{\,-1/2}\right]^k \tag{4.25}$$

By recalling that $W_b = \alpha\,\mathcal{V}_e\,C_0$, from Eq.4.22 the weight ratio for maximum endurance is

$$\left.\frac{W_b}{W_0}\right|_{me}^{(0)} = 2 \tag{4.26}$$

Note that this last result does not depend on rotor figure of merit. Thus, it can be used for addressing preliminary sizing of the platform according to mission requirements without the need for any detail on the rotor system. To this aim, Eq.4.1 is reshaped as

$$W_{to} = k_{eo}\,W_{to} + k_b\,W_{to} + W_p \tag{4.27}$$

where $k_{eo} = W_{eo}/W_{to}$ and $k_b = W_b/W_{to}$. Since payload weight, W_p, is usually defined as a requirement, the initial guess value for take-off weight is then given by

$$W_{to}^{(0)} = \frac{W_p}{1 - k_{eo} - k_b} \tag{4.28}$$

Parameter	Symbol	Value	Units
Airframe			
Number of rotors	n	6	
Airframe size	d_A	750	mm
Empty weight	W_{eo}	19.62	N
Payload weight	W_p	2.32	N
Avionics and payload power	P_{ap}	18	W
Rotor			
Motor parameter	K_v	700	rpm/volt
Motor size	d_e	31	mm
Propeller diameter	d_p	10	in
Propeller pitch	β	4.4	in
Figure of merit constant parameter	f_0	0.3814	
Figure of merit power parameter	m	0.1617	
Mean value 65-100%	f_{65}	0.4068	
Battery			
Voltage (fully charged/standard)	$\mathcal{V}_0, \mathcal{V}_f$	16.85 / 14.82	V
Nominal capacity	C_0	10-40	Ah
Rated discharge time	t_0	1	h
Weight/energy ratio	α	0.0509	N/Wh
Discharge fraction	η	0.71	
Peukert coefficient	k	1.051	

Table 4.2: Multi-rotor platform parameters

where k_{eo} is obtained from a statistical analysis of existing platforms, and k_b is chosen to be 2/3 according to Eqs.4.12 and 4.26.

4.1.6 Analysis and Results

The numerical model for hovering time prediction and approximate solutions describing the best endurance condition are applied to a 750 mm size six-rotors platform equipped with a 2-axis stabilized camera. Aircraft data and parameters relevant for the proposed applications are reported in Table 4.2 whereas Figure 4.7 shows the test platform.

Figure of merit model described by Eq.4.11 is first validated by means of a test rig for measuring the thrust delivered by the rotor and the power required for driving it. Figure

Figure 4.7: Multirotor platform used for validation

4.8 shows the data acquired for 13 different throttle settings between 40% and 100%. Model parameters, f_0 and m, are then obtained by a least-square estimate, and Fig. 4.9 presents measured and approximated figure of merit as a function of the throttle.

The proposed model provides an accurate fit up to 75 % of the throttle setting, whereas an increasing percentage error is found at higher values (5 @ 80 %, 8 @ 90 %, 10 @ 100 %). Nonetheless, for many multi-rotor platforms, the driving system is sized so that the power margin, intended as the ratio between the power available on-board and the power required at hovering, lies between 1.2 and 2.2 [7]. As a matter of fact, these values for the power margin allow for an increased maneuverability and, in case of a 6-rotor configuration, they allow for keeping the hovering condition with a residual manoeuvre capability even in case of engine failure. This makes the $50 - 70\%$ range suitable for operating the hovering flight condition.

On the basis of the model for figure of merit, multi-rotor endurance is computed as a function of battery ratio, W_b/W_0. Fig. 4.10 compares numerical prediction expressed by Eq.4.13 and approximate solutions derived in Section 2.1 with endurance calculated by using the measured values of figure of merit.

Results show how in the range where the figure of merit model fits the measured data, the hovering time prediction is accurate as well. At larger values of the throttle position,

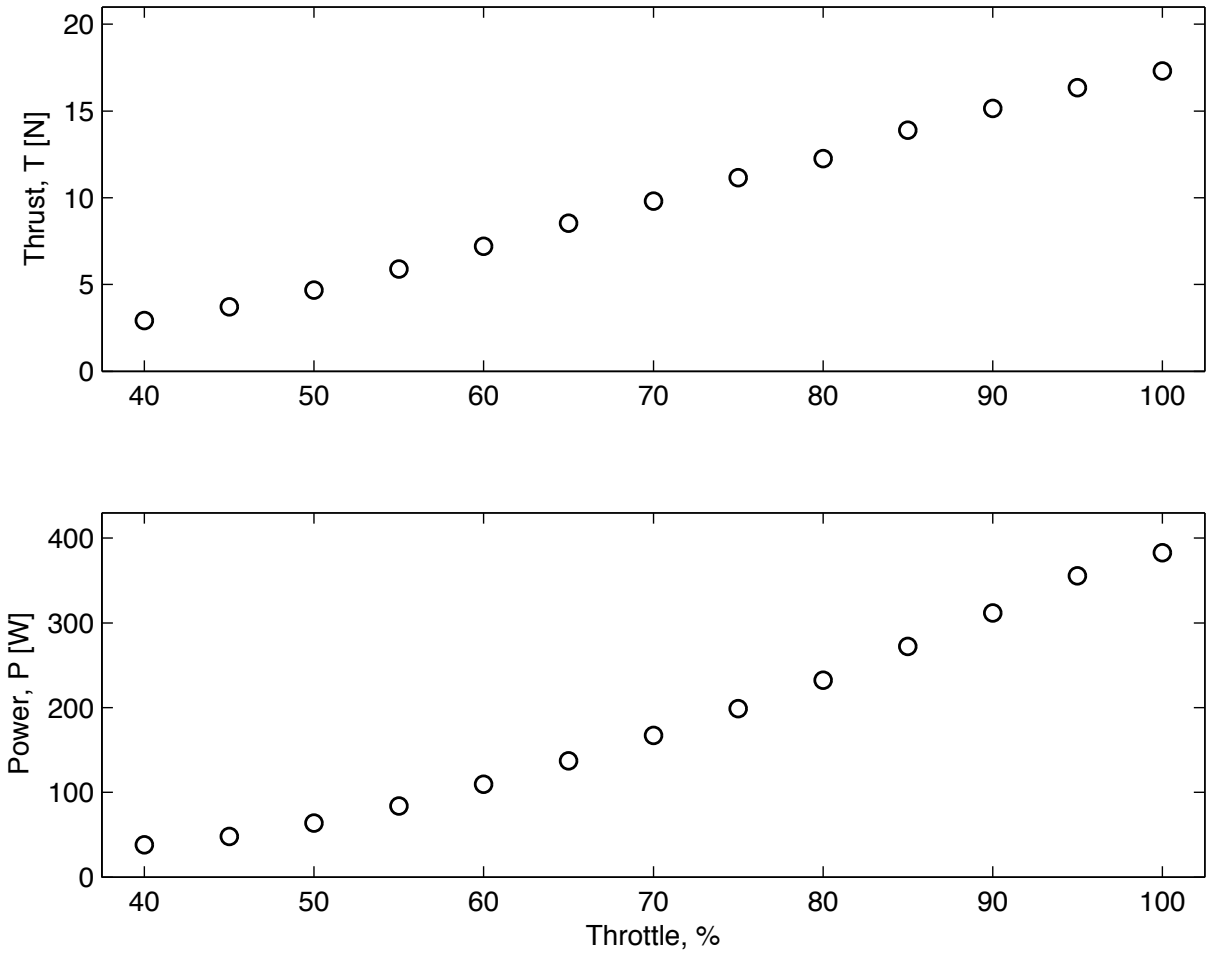

Figure 4.8: Measured rotor thrust and power as a function of the throttle

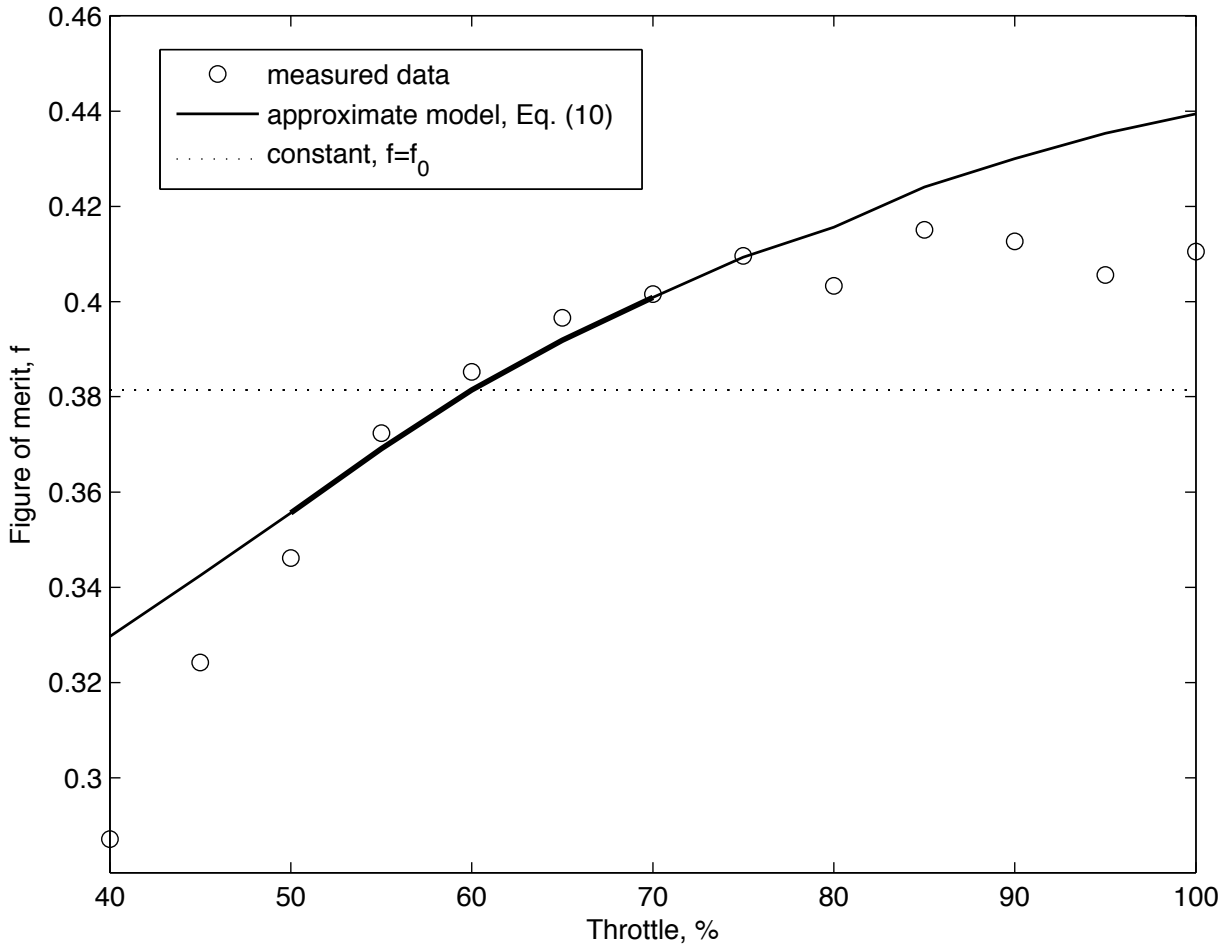

Figure 4.9: Rotor figure of merit as a function of the throttle

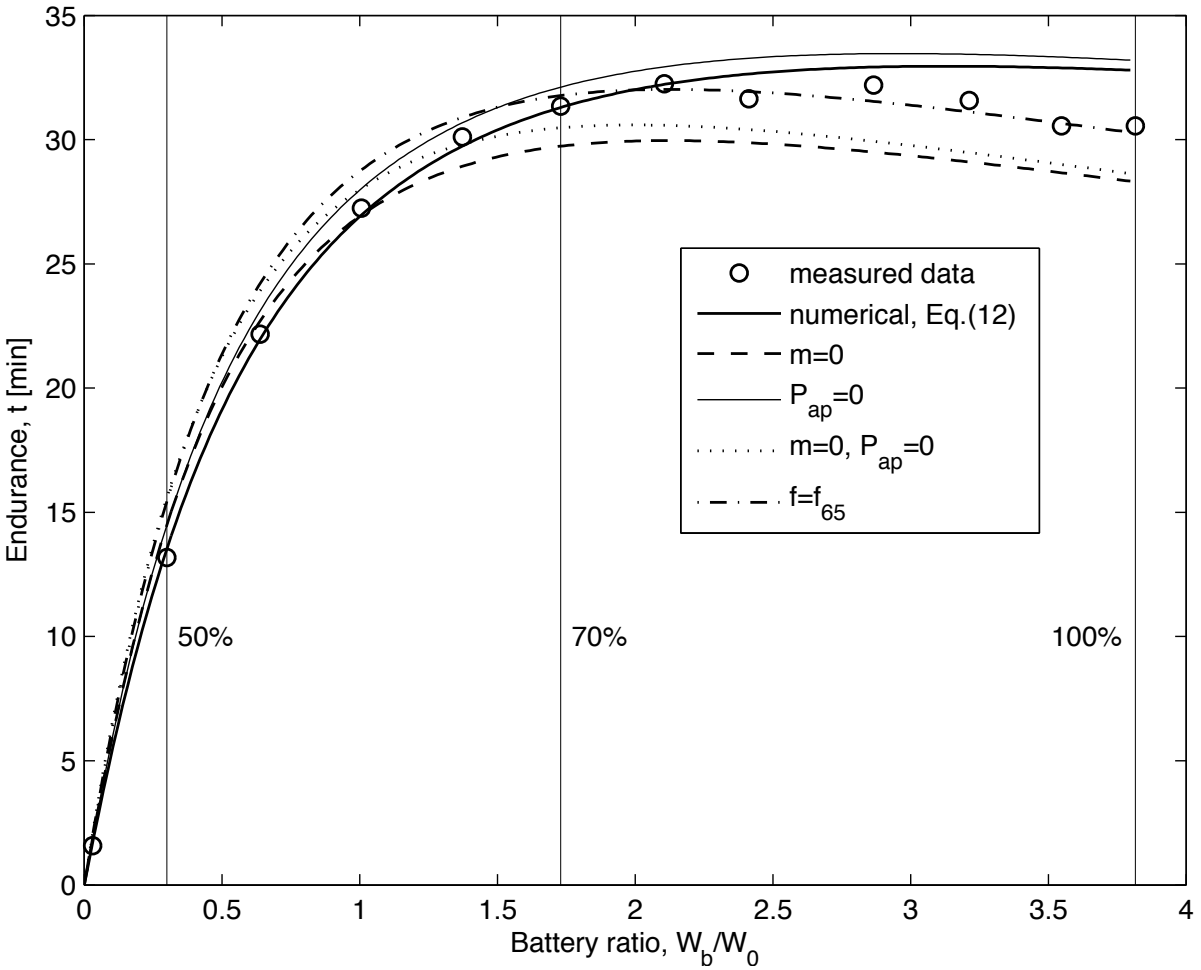

Figure 4.10: Hovering time as a function of the battery ratio

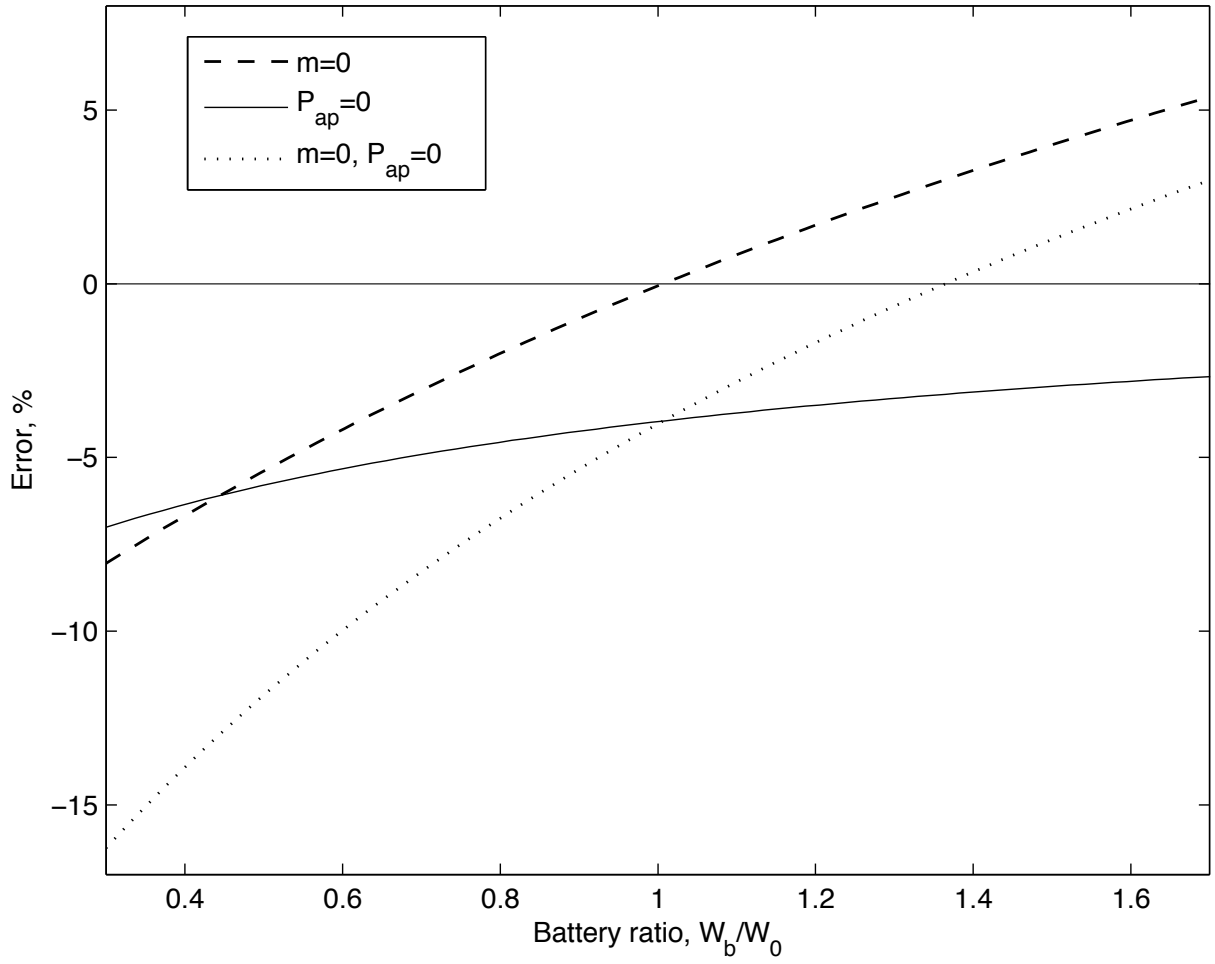

Figure 4.11: Endurance error of approximate models in the range 50-70% of the motor throttle

where the figure of merit model is affected by an increasing error, the estimation provided Eq.4.13 looses accuracy. Nonetheless, since the measured figure of merit exhibits small variations beyond the 65% throttle position, the hovering time can be estimated according to Eq.4.19 by using $f = f_{65}$, that is the mean value of figure of merit in the range 65 and 100%. This produces suitable estimates, especially for the best endurance battery ratio which is overestimated when Eq.4.13 is used.

Accuracy of approximate solutions in the range $50 - 70\,\%$ is highlighted in Fig. 4.11 in terms of the percentage error.

The model derived under the hypothesis of small payload required power provides, as expected, an overestimation of the hovering time in the whole range of the throttle, with a maximum error of $6\,\%$. On the other hand, under the hypothesis of constant figure of merit, the corresponding model shows a larger error, as high as $8\,\%$ far from the propeller

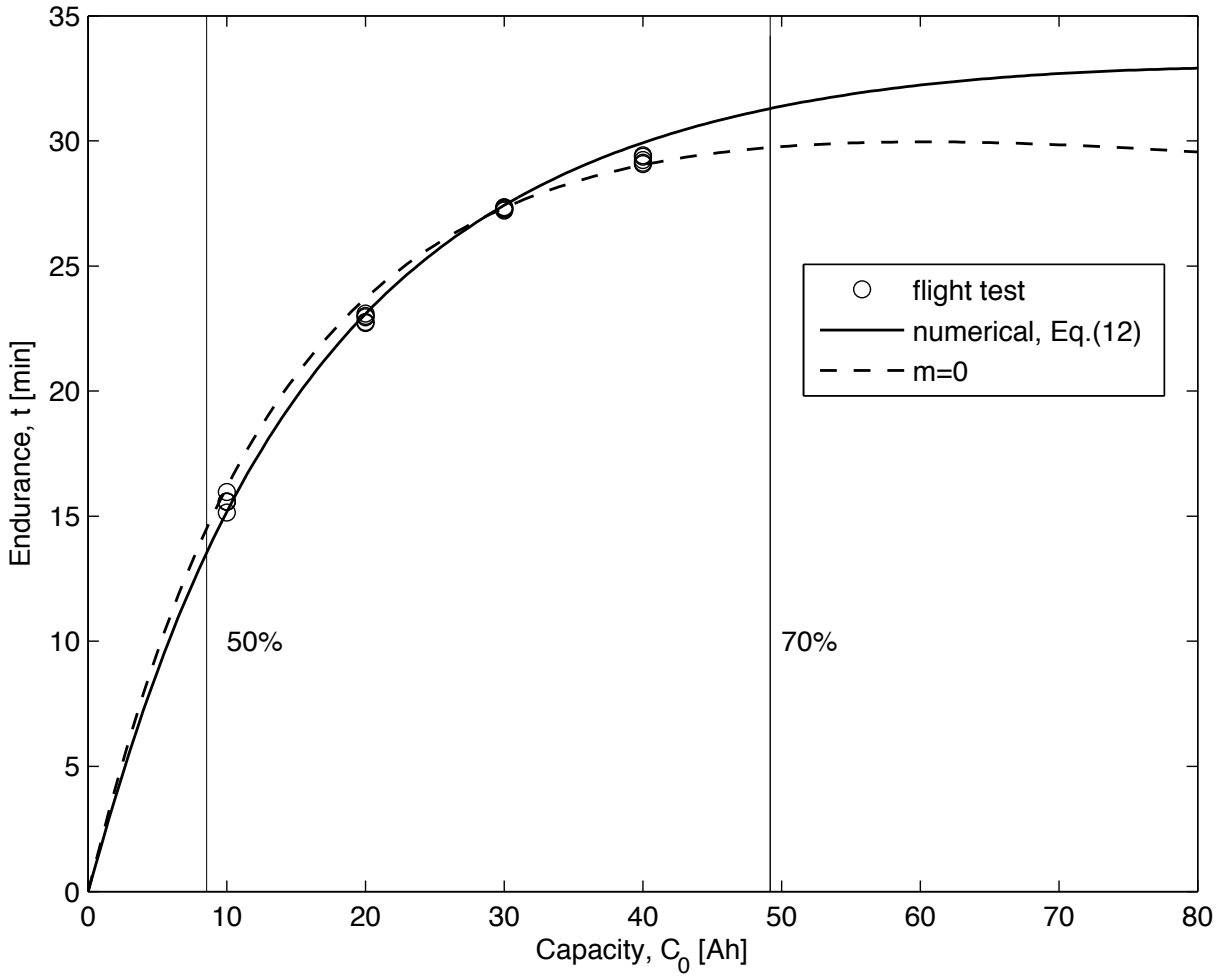

Figure 4.12: Experimental validation

regime where $f = f_0$, but it provides the exact estimation when the actual figure of merit lies in the neighborhood of f_0. Also, it is worth noting that the simplest approximate model, given by $m = 0$ and $P_{ap} = 0$, still provides an acceptable estimation of the hovering time, with a percentage error of about 15 % in the absence of detailed information on rotor and payload characterization.

To validate the proposed methodology, an experimental test campaign is performed. A total of twenty hovering flights are completed by using batteries with identical weight/energy ratio, α, along four different nominal capacity values. Figure 4.12 presents the experimental hovering time plotted vs. the nominal capacity.

Experimental data are compared to the analytical prediction of Eq.4.13 and constant figure of merit approximation of Eq.4.19. Statistics of the test campaign are provided in Tab.4.3 in terms of mean value, $\bar{t}$, and standard deviation, σ_t.

Results show how the proposed approach provides a satisfactory estimation of the hov-

Capacity [Ah]	**Take-off weight [N]**	**Endurance [min]**		
		Eq.(12)	Experimental	
C_0	W_{to}	t	$\bar{t}$	σ_t
10	29.20	15.12	15.57	0.2902
20	36.84	22.90	22.86	0.1630
30	44.49	27.42	27.28	0.056
40	52.13	29.90	29.24	0.1522

Table 4.3: Experimental results

ering time, making the model a suitable analytical tool for the preliminary design phase. In this respect, it is important to note that following an increase of battery capacity, the corresponding increase in hovering time shows a negative trend. By increasing the capacity from 10 to 20 Ah, one gains about 10 minutes of hovering time, for the considered platform, which largely increases the initial endurance. A further addition of 10 Ah increases endurance by less than 5 minutes. A further increase from 30 to 40 Ah provides only 2 minutes of additional hovering capability. These data represents a further proof for the importance of correctly addressing the issue of preliminary sizing the battery-powered aircraft, especially for multi-rotor platforms, on the basis of a physically sound methodology. As a matter of fact, trying to increase the endurance of an already existing platform by simply adding batteries may not be an effective solution, as propeller operates at higher motor regimes, where the decreasing slope of the endurance vs. capacity plot provides only a marginal improvement.

Bibliography

[1] Harwin S., Steve and Lucieer A.,*Assessing the Accuracy of Georeferenced Point Clouds Produced via Multi-View Stereopsis from Unmanned Aerial Vehicle (UAV) Imagery*, Journal of Remote Sensing, Vol.4, No. 6, 2012

[2] Rudol P., Doherty P., *Human Body Detection and Geolocalization for UAV Search and Rescue Mission Using Color and Thermal Imagery* Aerospace Conference, Big Sky, MT, 2008 IEEE, 1-8 March 2008

[3] Casber D.W., Beard R.W., McLain T.W., *Forest Fire Monitoring With Multiple Small UAVs*, 2005 American Control Conference, June 8-10, 2005. Portland, OR, USA

[4] Traub L.W., *Range and Endurance Estimates for Battery-Powered Aircraft*, Journal of Aircraft Vol. 48, No. 2, March-April 2011

[5] Avanzini G., Giulietti F., *Maximum Range for Battery-Powered Aircraft*, Journal of Aircraft Vol. 50, No. 1, March-April 2013

[6] Traub L.W., *Validation of endurance estimates for battery powered UAVs*, Aeronautical Journal Vol. 117, No 1197, November 2013

[7] Verbeke, J., Hulens, D., Ramon, H., Goedemé, T., De Schutter, J.; *The Design and Construction of a High Endurance Hexacopter suited for Narrow Corridors*, ICUAS, 27-30 May 2014, Orlando, FL, USA.

[8] Roskam, J., *Airplane Design. Part VII: Determination of Stability, Control and Performance Characteristics: FAR and Military Requirements*, University of Kansas, Lawrence (KS), 1986, Chap. 5.

[9] Raymer, D.P., *Aircraft Design : a Conceptual Approach*, 4th ed., AIAA, Reston (VA), 2006, Chap. 17.

[10] Gatti M., Giulietti F., *Preliminary Design Analysis Methodology for Electric Multirotor*, RED-UAS 2013,2nd IFAC Workshop on Research, Education and Development of Unmanned Aerial Systems, November 20-22, 2013, Compiegne, France.

[11] Leishman, J. Gordon, *Principles of helicopter aerodynamics, 2nd Ed.*,Cambridge University Press, Cambridge Aerospace Series, 2000, Cambridge, New York.

[12] Doerffel, D., Sharkh, S.A.; *A critical review of using Peukert equation for determining the remaining capacity of lead-acid and lithium-ion batteries*, Jurnal of Power Sources 155 (2006)395-400.

[13] Shepherd C. M.,*Design of Primary and secondary Cells*, Journal of The Electrochemical Society Vol. Vol. 112, 1965

[14] Tremblay O., Dessaint L.A.; *Experimental Validation of a Battery Dynamic Model for EV Application*, World Electric vehicle Journal Vol.3 -ISSN 2032-6653 - (2009 AVERE)

[15] Gundlach, J. (2012). Designing Unmanned Aircraft Systems: A Comprehensive Approach (1 ed.). Virginia: AIAA Education series.

[16] Brandt, S. A., & Gilliam, F. T. (1995, July-August). Design Analisys Methodology for Solar-Powered Aircraft. Journal of Aircraft, 32(4).

[17] Hanselman, D. C. (n.d.). Brushless Permanent-Magnet motor Design. New York: McGrave-Hill.

[18] Ohad, G., & Aviv, R. (2009, Julay-August). Optimizing Electric Propulsion Systems for Unmanned Aerial Vehicles. Journal of Aircraft , 46(4).

[19] Prouty, R. W. (2002). Helicopter Performance, Stability, and Control . Malabar - Florida: Krieger Publishing Company, inc.

[20] Shiau, J.-K., Der Ming, M., Chih-Wei, C., & Jie-Ren, S. (2010, March-April). Optimal Sizing and Cruise Speed Determination for a Solar-Powered Airplane. Journal of Aircraft, 47(2).

[21] Brandt J.B., Selig M.S., *Propeller Performance Data at Low Reynolds Numbers*, University of Illinois, Urbana, 2011, 49th AIAA Aerospace Sciences Meeting, AIAA 2011-1255

[22] MIT Electrical Vehicle Team, *A Guide to Understanding Battery Specifications*, December 2008

[23] Coleman P.C., *NASA TR 3675 - A Survey of Theoretical and Experimental Coaxial Rotor Aerodynamic Research*, Ames research Center, Moffett Field, california, 1997

[24] Shepard C.M., *Theoretical Design of Primary and Secondary Cells - Part III - Battery discharge equation* , NRL Report 5908, US Naval research Laboratory, Washington DC, May 2, 1963

[25] tremblay O., Dessaint L.A., *Experimental Validation of a Battery Dynamic Model for EV Application*, Electric Vehicle journal Vol. 3, ISSN 2032-6653, 2009 AVERE

[26] Jung-Ki Park, *Principles and Applications of Lithium Secondary Batteries*, Wiley, ISBN: 978-3-527-33151-2, August 2012

[27] Jha A.R. *Next-Generation Batteries and Fuel Cells for Commercial, Military, and Space Applications*, CRC Press - Taylor and Francis Group

[28] *Handbook of Batteries*, D. Linden - T.B. Reddy Editor, 3th Edition, McGraw-Hill